MEDIUM-PRESSURE METAMORPHISM IN THE CENTRAL SANTANDER MASSIF, EASTERN CORDILLERA, COLOMBIAN ANDES

García, C. A.[1]; Ríos, C. A.[1]; and Castellanos, O. M.[2]

ABSTRACT

The Central Santander Massif exposes its metamorphic basement, which mainly consists of medium- to high-grade pelitic schists, paragneisses, migmatites and orthogneisses. For delineating its metamorphic evolution, we have examined mineral assemblages, metamorphic reactions and P-T conditions of metamorphic rocks of this region. Metamorphism has occurred under conditions of high-temperature and medium-pressure (Barrovian type metamorphism), and three metamorphic zones were developed: staurolite-kyanite, sillimanite and migmatite zones. Pressure and temperature conditions, estimated by TWQ program, are in the range of 5.0-9.5 kbar and 630-727°C. The P-T path of the metamorphic units is clockwise suggesting a collision model for this region of the Colombian Andes.

Keywords: Metamorphism; Santander Massif; Barrovian type; P-T path; collision

METAMORFISMO DE PRESION INTERMEDIA EN LA REGION CENTRAL DEL MACIZO DE SANTANDER, CORDILLERA ORIENTAL, ANDES COLOMBIANOS

RESUMEN

La región central del Macizo de Santander expone su basamento metamórfico, el cual consiste de esquistos pelíticos, paraneises, migmatitas y ortoneises de medio a alto grado. Para delinear su evolución metamórfica, hemos examinado las paragénesis minerales, reacciones metamórficas y condiciones de P-T de las rocas metamórficas de esta región. El metamorfismo ocurrió bajo condiciones de alta temperatura y presión intermedia (metamorfismo tipo Barroviano), con el desarrollo de tres zonas metamórficas: estaurolita-cianita, silimanita y migmatita. Las condiciones de presión y temperatura, estimadas mediante el programa TWQ, están en el rango de 5.0-9.5 kbar y 630-727°C. La trayectoria de P-T de las unidades metamórficas es en sentido horario sugiriendo un modelo de colisión para esta región de los Andes Colombianos.

Palabras claves: Metamorfismo; Macizo de Santander; tipo Barroviano; trayectoria de P-T; colisión.

[1] Escuela de Geología, Universidad Industrial de Santander, A. A. 678, Bucaramanga, Colombia.
[2] Universidad de Pamplona, Pamplona, Colombia.

INTRODUCTION

The Santander Massif is located into the northern part of Eastern Cordillera of the Colombian Andes. The basement of this massif is composed by igneous and metamorphic rocks, which reflect a complex geological history. During the last years, the Santander Massif metamorphic rocks have been studied to know their mineral compositions, textural and microstructural features, mineral chemistry and thermobarometric estimates. Some of these studies have been focused to determine the tectono-metamorphic evolution of the southwestern Santander Massif region, which has constitued a valuable contribution for interpretation of geologic and tectonic evolution of the northwestern continental margin of South America.

The purpose of this paper, which is concerned with the description of a high-T and medium-P facies series of the central Santander Massif, is to determine the P-T path followed by the metamorphic basement. The reconstruction of the tectono-metamorphic evolution of these metamorphic rocks is based on the detailed petrographical study, reaction history, chemistry of the constituent minerals, and geothermobarometry, and the results of this are very important to understand the evolution of orogenic processes of the Andes.

GEOLOGICAL SETTING

The Santander Massif is situated in the northeastern part of Colombia (FIGURE 1). The basement complex of the
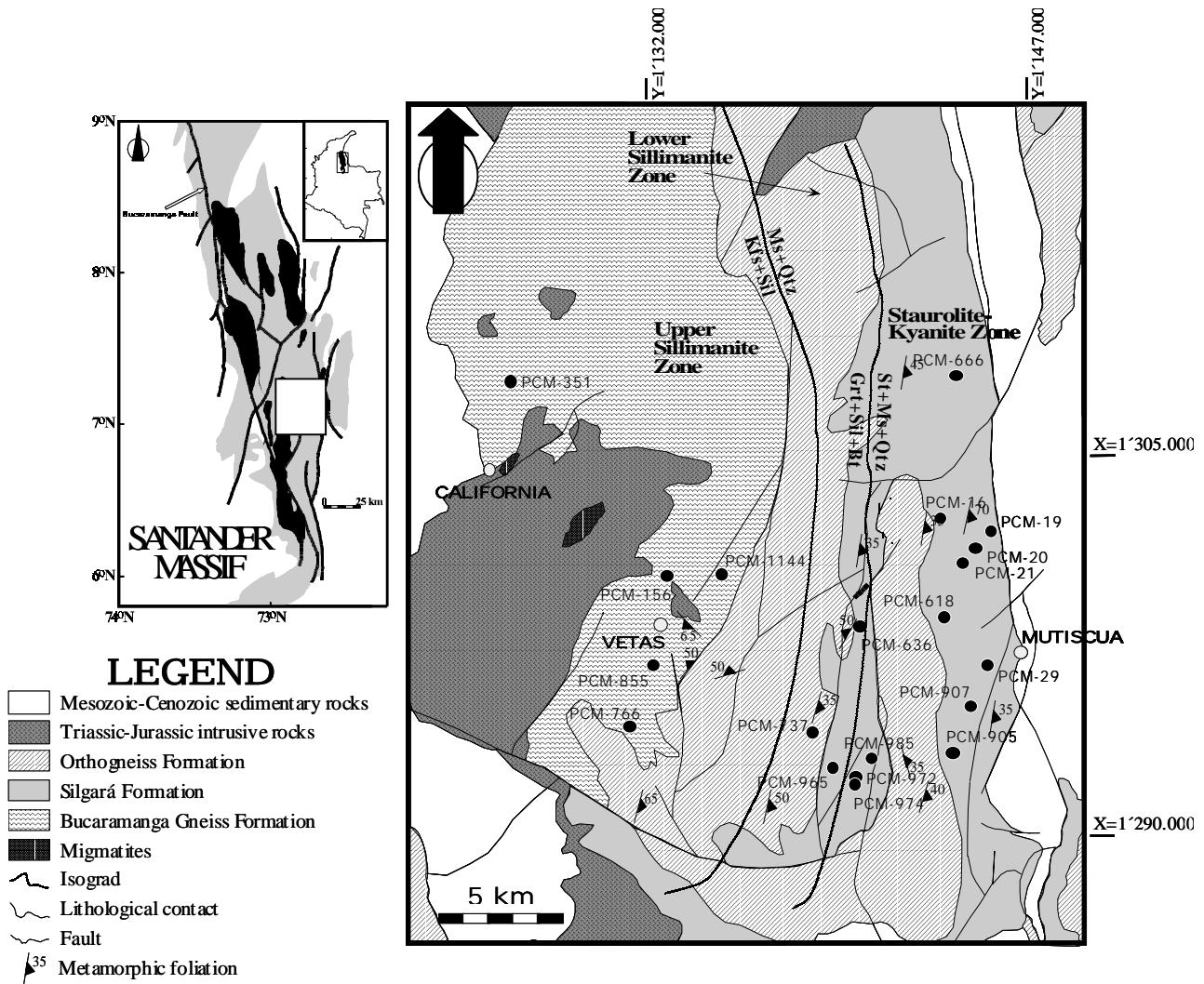

FIGURE 1. Generalized geological map of the Santander Massif (left side), showing the distribution of the metamorphic (grey colour), igneous (black colour) and sedimentary (white colour) rocks modified after Goldsmith et al. (1971), as well as the study area, and geological map of the central Santander Massif (right side) modified after Ward et al. (1973).

Santander Massif comprises metamorphic rocks of pre-Devonian age, which are cut by intrusive bodies of Triassic to Cretaceous ages (e.g. Goldsmith, 1971; Boinet *et al.* 1985), although age of several igneous bodies is still under debate, due to scarce isotopic data. The metamorphic rocks of this basement have been divided into three units from bottom to top Bucaramanga Gneiss (BG), Silgará Formation (SF), and Orthogneiss (O). The basement of the Santander Massif is unconformably overlain by unmetamorphosed rocks of the Floresta Formation. Carboniferous and Permian clastic to calcareous sediments unconformably overlain this unit. However, due to pre-Cretaceous erosional events, the occurrence of these sequences is restricted. Triassic sedimentary rocks of the Tiburón Formation overlay these sequences. Post-Paleozoic sediments, which overlay the Upper Paleozoic marine sediments, include the Bocas and Jordán formations. The latter consists of fine-grained red beds with interlayered volcanic rocks and intrusive clasts, which is discordantly overlain by the red bed sequence of the Girón Formation of Jurassic age. Cretaceous sedimentary rocks occur around the Santander Massif and are preserved as erosional relics.

The first study on the geology of the Santander Massif was done by Julivert (1958, 1959, 1961a, 1961b, and 1963, 1970), and later described in detail by Ward *et al.* (1973). Most of the previous studies have used mainly geological, structural, paleontological or isotopic data to decipher the evolution of the Santander Massif. Structural studies in the Santander Massif have been generally related to stratigraphic work. Julivert (1970) discusses mainly the relationships between basement and sedimentary cover, since these determine the main structural features of the Eastern Cordillera.

The Santander Massif is a structurally uplifted block, limited to the west by the Bucaramanga - Santa Marta Fault and to the east by the fault system Pamplona - Cubogón - Mercedes. According to Ward *et al.* (1973), in the Santander Massif the foliation and fold orientations are approximately similar in the BG, SF and O metamorphic rocks. Regionally, these orientations are N-S, and tend to be parallel to the axis of the orogenic belt (Eastern Cordillera), showing local variations and discontinuity because of the presence of intrusive bodies of the Santander Plutonic Complex and covering of sedimentary rocks. Restrepo-Pace (1995) proposes for the Santander Massif fault system a shear-couple model. The model requires left lateral sense of shear along bounding faults i.e. the Bucaramanga Fault on the west and the Pamplona thrust-front on the east, the development of northwesterly trending antithetic faults, counterclockwise rotation of rigid internal blocks and inversion of Mesozoic NS trending extensional structures.

The first study on the metamorphism of the Santander Massif was done by Ward et al (1973). Studies based on a collecting of information about the distribution of facies of metamorphism in Colombia are presented by Maya, 1997. More recent works (e.g., Restrepo-Pace, 1995; Schafer *et al.* 1998; García y Ríos, 1997; García y Castellanos, 1998; Ríos, 1999; Ríos and Takasu, 1999; García y Ríos, 1999; García y Campos, 2000; Castellanos, 2001; Ordoñez; 2003; Ríos *et al.* 2003; Cardona, 2003) have placed considerable reliance in the results of mineralogical, petrographical, geochemical, thermobarometric, and geochronological studies of the metamorphic rocks in different regions of the Santander Massif.

The metamorphic sequence exposed in the study area, which is extended from California to Mutiscua, corresponds to the CSM. A generalized geological map of the study area is shown in FIGURE 1. The oldest lithologic unit in the CSM corresponds to the BG that crops out between California and Vetas towns and is a sequence consisting of pelitic and mafic gneisses, with subordinate amounts of amphibolites, migmatites which was metamorphosed to high grade. The SF, a younger and overlying unit, is a middle- to high-grade metamorphic sequence, which consists of metapelitic rocks with intercalations of metamafic, quartzfeldspar and metacarbonate rocks. It partially envelops the BG and O units and crops out from southern part of Berlin towards the north, as well as to the west of the Mutiscua Fault. Its lithology changes in composition to the west, from top to bottom, from marble through different varieties of mica schist to quartzite. The O unit occurs to the southwest, north and northeast of Berlín, and is highly distributed in the middle- and high-grade metamorphic rocks. It consists on quartz-feldspar and biotite gneiss and generally shows concordant foliation and lineation with those of neighboring of the BG and SF metamorphic rocks. The contact between the Silgará Formation and the Orthogneiss is intrusive, which evidence the emplacement of orthogneiss masses. The contact relationship between the BG and SF metamorphic rocks is unclear but is probably an unconformity (Ward *et al.*, 1973).

The most important structural feature in the CSM (Páramo de Santurbán) is represented by a broken gneiss dome. The SF dips separating from this dome on the eastern part and surrounds the BG and O units in the southern

part. The foliation in the BG strikes from NE to NW, changing suddenly. For example, near to Vetas it is defined a general pattern of direction NE, dipping 60-85°SE. It dips to the west on the western part and dips to the east on the central part of the study area, and it is possible that this reflects a folding structure. On the other hand, the foliation is also defined by a preferred orientation NE in the SF and O metamorphic rocks, because in the SF it strikes N15-20°E, dipping 30-35°SE, whereas in the O it strikes N15-18°E, dipping 30-40°SE, which is in agreement between these metamorphic units and could reflect a common metamorphic event for them.

PETROGRAPHY

A detailed petrographic study of thin sections was carried out on specimens collected in the CSM to ascertain both mineral assemblages and textural and microstructural features in the metamorphic rocks. The petrography study was developed in the Geology Research Laboratory of the Universidad Industrial de Santander, Guatiguará Research Center (Colombia). The studied metamorphic rocks of the study area are described below. FIGURE 2 illustrates the main petrographical aspects of the metamorphic rocks in the CSM. Mineral abbreviations are after Kretz (1983).

Bucaramanga Gneiss (BG)

The BG comprises *pelitic* (biotite gneisses), *mafic* (hornblende gneisses, biotite-hornblende gneisses and amphibolites), and *quartzfeldespathic* (quartzfeldspar gneisses and quartzites) *rocks*, which show a banded aspect. The pelitic and mafic rocks predominate in this metamorphic unit. Gneisses are the more common rocks in this unit and their main minerals are quartz, plagioclase, potasium feldspar, as well as sometimes biotite, hornblende or sillimanite. Garnet and sometimes biotite, hornblende or sillimanite constitute minor minerals. Common accesory minerals are sphene, rutile, Fe-Ti oxides, garnet, zircon and apatite. Quartzfeldespathic rocks are interlayered into the pelitic rocks; they are quartzfeldspar-rich rocks with subordinate amounts of garnet, sillimanite, biotite and muscovite, and accesory minerals such as zircon and apatite. A granoblastic texture is mainly dominant, and a lepidogranoblastic texture sometimes occurs. The mafic rocks show a banded to massive structure and correspond to gneisses with major minerals such as hornblende and biotite, which predominate on quartz and feldspar. Muscovite is a minor mineral. Accesory minerals are sphene, zircon and apatite. Amphibolites contain hornblende and plagioclase, while quartz, biotite, sphene and apatite are minor or accesory minerals. The dominant texture in these rocks is granoblastic or nematogranoblastic. The compositional and textural varieties of gneisses are not cartografiables, and they are interlayered into the metamorphic sequence.

Metapelites from the migmatite zone show a banded, microfolding or nebulitic structure characterized by a gneissic layering defined by millimetre-scale alternating micaceous and quartzfeldespathic domains. They sometimes vary in composition from biotite-bearing migmatite to hornblende-bearing migmatite and are mainly composed by quartz, plagioclase, potasium feldspar, biotite, and hornblende, with minor epidote and opaque minerals. The quartzfeldespathic domains have a coarse-grained granitic mineralogy and form continuous layers or small boudinaged pods, and the granitic leucosome could represent the in situ segregation of the melt, whereas the micaceous domains are composed by biotite or hornblende, fibrolitic sillimanite and sometimes minor muscovite. Fibrolitic sillimanite sometimes forms elongated whitish nodules up to 1.5cm in size parallel to the stretching lineation, which can be interpreted as being due to partial melting.

Silgará Formation (SF)

The SF is composed of a metamorphic sequence, which is characterized by interlayered pelitic schists and mafic rocks, and displays a well-developed schistosity. The most obvious structure in these rocks is a dominant schistosity or slaty cleavage, which may be developed at the same time with the first-generation of folds and thrusts or superimposed upon older structures. In general, later structures such as flat-lying crenulations, small chevron folds and kink bands overprint the main foliation. The SF in the study area comprises four petrochemical types of metamorphic rocks: *pelitic*, *semipelitic*, *mafic* and *carbonate rocks*, which are described below.

Pelitic rocks (feldspar-micaschists and micaschists) are the major constituents of the Silgará Formation in this area, showing a schistose or sometimes slaty cleavage structure. They contain muscovite, biotite, quartz and plagioclase as major minerals. The modal contents of staurolite and sillimanite changes highly and these minerals become to be accesory or major phases. Garnet and opaque minerals are minor minerals, and tourmaline, kyanite, graphite, sphene; zircon and apatite are accesory minerals. Andalusite or kyanite sometimes occurs as a minor phase and plagioclase occurs as a minor or accesory phase, although this mineral could be absent. These rocks display a granolepidoblastic to porphyroblastic (in a
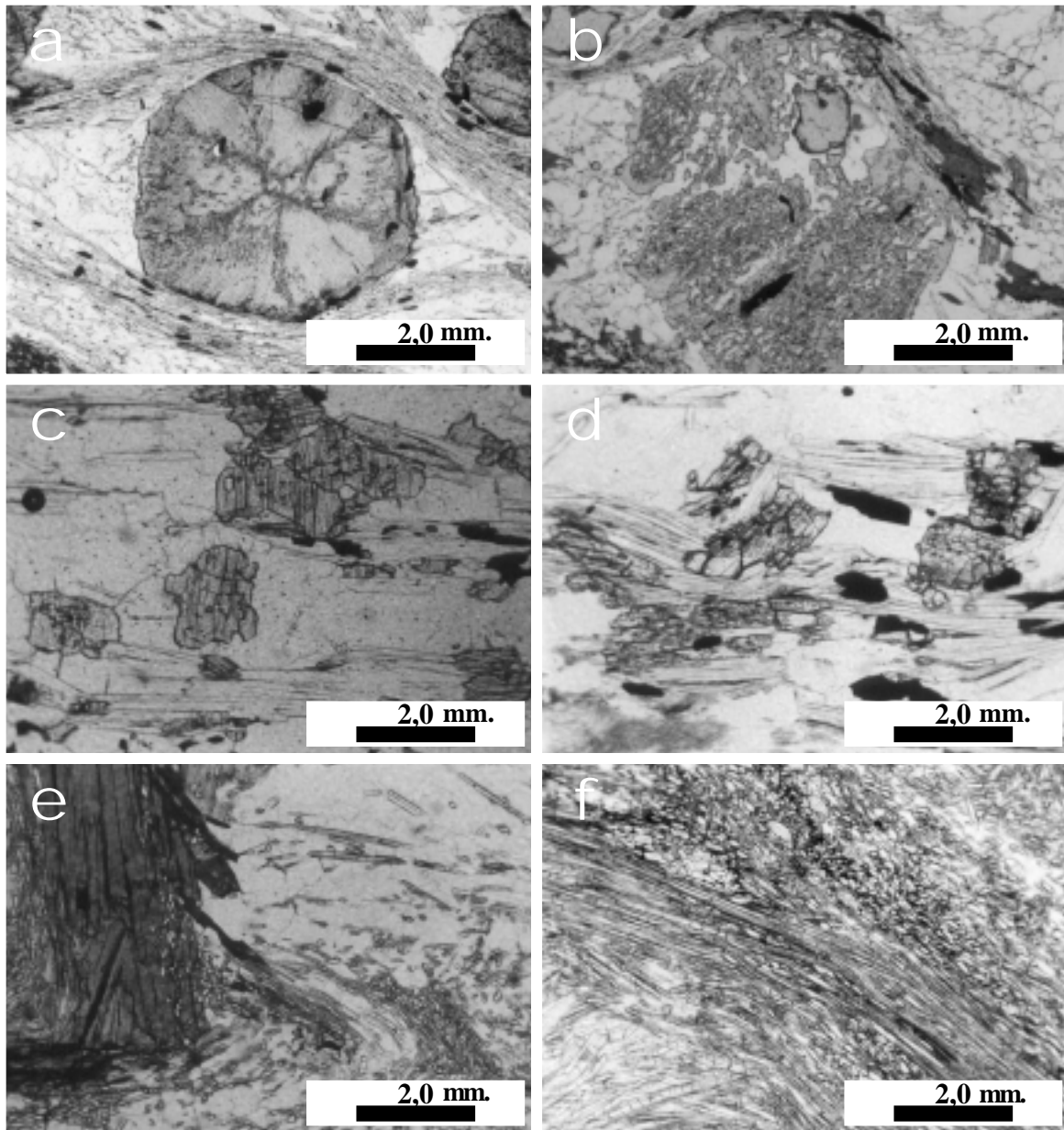
FIGURE 2. Main petrographic features in metamorphic rocks of the central Santander Massif. (a) Garnet porphydoblast displaying sector zoning due to the concentration of inclusions in interfacial borders. Observe the assymetrical pressure shadow around garnet. (b) Relict of garnet as inclusion in staurolite porphydoblast, which shows numerous quartz inclusions that define an internal schistosity (S_{int}) discordant with the main fabric of the rock (S_{ext}). (c) Kyanite crystals showing high relief, well-developed and marked cleavaje and partition parallel to (001) approximately to straight angles with the lenght of the crystals. (d) Fibrolitic sillimanite growing after kyanite crystals. (e) Microcrenulated structure in biotite-sillimanite gneiss, in which sillimanite appears to be developed after biotite reeplacement. (f) Prismatic sillimanite, in which some crystals are cut perpendicular to their lenght and show diamond-shape cross sections with cleavaje after (010).

granolepidoblastic matrix) texture. They often show macroscopically recognizable garnet and staurolite porphyroblasts, which contain abundant inclusion trails forming an internal foliation, although andalusite or kyanite porphyroblasts sometimes occur in these rocks. Internal foliation in staurolite and/or garnet is marked by quartz and ilmenite inclusions and is continuous with the external foliation of the rock, which is defined by biotite and muscovite. Rotation of the internal foliation in staurolite and/or garnet porphyroblasts indicates a dextral or sinistral sense of shearing.

Semipelitic rocks comprise quartz-feldspar schists, mica-quartz schists, feldspar quartzites, mica-feldspar quartzites, muscovite quartzites and feldspar quartzites and show a schistose, banded or massive structure. Quartz, muscovite and sometimes plagioclase, andalusite and kyanite are major phases. Minor minerals are garnet, muscovite, andalusite or kyanite, and ocasionally biotite and opaque minerals. The accesory minerals are tourmaline, sphene, zircon, apatite, epidote and/or clinozoisite, and biotite. These rocks show a porphyroblastic (in a lepidogranoblastic matrix) texture, although it is locally lepidogranoblastic or granoblastic. Plagioclase, staurolite, garnet and andalusite or kyanite porphyroblasts commonly occur, although in variable modal contents, sometimes with quartz and muscovite inclusions, producing a poikiloblastic texture. *Mafic rocks* (amphibole schists and biotite-amphibole schists) occur as thin layers in the contact between marble and semipelitic rocks. The major minerals in these rocks are hornblende and quartz, whereas epidote and garnet can be minor or accesory phases. They may represent dykes and sills emplaced prior to deformation and metamorphism. Schäfer *et al*. (1998) carried out a study on petrology and geochemistry of the mafic rocks of the SF in the southwestern Santander Massif, according to these authors, the content of major and trace elements indicate a magmatic origin for these rocks.

Carbonate rocks are represented by marble, which shows a massive structure and they are mainly composed by calcite, which is a major mineral, with subordinate amounts of quartz, epidote and zoisite that, in general, do not reach the 2 % modal content of these rocks.

Orthogneiss (O)

This metamorphic unit comprises *mafic* (biotite-hornblende gneisses) and felsic (quartz-feldspar gneisses) *rocks*. The mafic rocks show a massive structure or a poorly developed foliation. They are hornblende-rich rocks with plagioclase and biotite as major mineral phases. Quartz is a minor mineral, and epidote and apatite are accessory minerals. The felsic rocks show a gneissose and, sometimes, augen structure. Quartz and feldspar are the main mineral phases, reaching more than the 95 % modal content of these rocks. Microcline and plagioclase are the dominant feldspar and their modal content is variable. Minor minerals are hornblende and biotite, although these minerals can be absent. Accesory minerals are zircon, apatite, epidote, clinozoisite and sphene. These rocks commonly display a lepidogranoblastic texture with biotite showing a preferred orientation following the main foliation of the rock. However, they sometimes display a granoblastic texture. Pertitic microcline usually occurs in these rocks.

MINERAL ASSEMBLAGES

TABLE 1 shows the different mineral assemblages in the metamorphic rocks at CSM, being the metapelitic rocks the most important lithology in the study area.

According to the mineral assemblages in pelitic and semipelitic rocks of the CSM, these rocks belong to the staurolite-kyanite and sillimanite zones of the Barrovian zonal scheme, which have defined the regional thermal structure of the metamorphic rocks in the study area, although a migmatite zone is locally observed (FIGURE 1). Barrovian metamorphism is a common, widespread, large scale metamorphism typically associated with major orogenic (mountain building) events. The metamorphic zones are related to regional dynamothermal metamorphism. The boundary of the metamorphic zones are defined by the first appearance of the index minerals in pelitic rocks, although the term reaction-isograd is preferred better than isograd, because a reaction-isograd will provide a better petrogenetic information, taking into account that it is bracketed by reactants and products, and may produce information about conditions of metamorphism. Textural observations show that andalusite is the earliest Al_2SiO_5 polymorph, kyanite is present at peak metamorphic pressure, whereas sillimanite is present at peak metamorphic temperature, the andalusite→kyanite and kyanite→sillimanite transformations occur; staurolite+kyanite coexist in the peak pressure assemblage in pelitic rocks of the Silgará Formation.

TABLE 1. Typical mineral assemblages in the metamorphic rocks at CSM.

Pelitic rocks	Semipelitic rocks	Mafic rocks	Carbonate rocks
Grt + Bt + Ms + St + Qtz ± Ky	Pl + Bt + Ms + Qtz	Hbl + Pl + Qtz	Cal + Qtz
Bt + Ms + Qtz ± Grt + St	Pl + Ms + Grt + Qtz + St	Grt + Hbl + Qtz	
Bt + Ms + Ky + Pl + Qtz	Pl + Mic + Qtz + Ms + Bt	Grt + Hbl + Pl + Bt + Qtz	
Ms + Ky + Qtz		Hbl + Pl + Qtz	
Grt + Bt + Ms + Sil + Qtz			
Grt + Bt + Sil + Kfs + Pl + Qtz			

In the CSM it appears that one regional metamorphism with distinct phases occurred. The metamorphic grade increases from lower amphibolite facies in the eastern part of the CSM to upper amphibolite facies with Sillimanite + K-feldspar + biotite - bearing assemblages (migmatization) in the western part of the CSM.

RELATIONSHIP BETWEEN METAMORPHISM AND DEFORMATION

Combined field, petrological and structural data indicate that the CSM is a structurally complex metamorphic terrain, where structural geometry is generally the result of complex polyphase deformation. The microstructural analysis has been developed on metapelitic rocks of the Silgará Formation, which is an excellent example of a Barrovian metamorphic sequence that provided important information to analyze the deformation history because diagnostic mineral assemblages from different tectonic events are preserved.

Microstructural evidence shows that the Silgará Formation metamorphic rocks at the CSM underwent prograde metamorphism during at least three deformation phases (D_1, D_2, and D_3), and extensive retrograde metamorphism during the last stage, and many of the retrograde mineral changes involve hydration. A polymetamorphism is suggested by the presence of multiple foliations and by garnet or staurolite porphyroblasts, which have complex time relations are post-tectonic to one foliation but pre-tectonic to another, or by a mineral phase, which has different forms or time relations in different crystals. The presence of these porphyroblasts let to examine earlier stages in the deformation history than that preserved in the matrix foliation. Numerous porphyroblasts of garnet, staurolite, biotite and/or muscovite are present in most outcrops, and can be shown to have grown post-tectonically to D_1 or D_2.

The first deformation phase D is the oldest that can be observed in the study area, although there is not a clear relationship between deformation and undeformed rock. During this phase, as a result of crustal shortening and thickening, the CSM metamorphic rocks were affected by a prograde metamorphism, developing S_1, which is recorded by the mineral assemblage quartz + ilmenite + graphite ± muscovite both as inclusion trails in garnet or staurolite porphryroblasts, and as a differentiated layering in D_2 hinge zones, defined by alternating layers of sheet-silicate and quartz-feldspathic minerals.

Deformation D_2 due to heating and thrusting developed progressively two foliations (S_2 and S_3) through medium pressure conditions. The S_2 schistosity, which is represented by the mineral assemblage quartz + muscovite + biotite + ilmenite + garnet + staurolite + kyanite ± andalusite ± plagioclase, is parallel to axial planes of isoclinal folds in intercalated quartz-feldspar-rich and phyllosilicate-rich layers, and represents the main regional foliation can be recognized through all metamorphic zones. The S_3 schistosity, which is represented by the mineral assemblage quartz + muscovite + biotite + staurolite, is younger than the S_2 schistosity (visible as a crenulated surface between layers of S_3). From pre-kynematic crystals of biotite, muscovite and quartz, and the Sin-S_2 pressure shadows that they develop, which do not show any internal schistosity, it is possible to consider that these minerals formed part of the S_1 schistosity. The presence of sigmoidal and pre-kynematic crystals and the development of asymmetrical pressure shadows and strain cap around these crystals, are interpreted as a process of deformation by rotation by which pressure shadows have been enriched in soluble minerals such as quartz, while the schistosity S_2 has been enriched in minerales such as muscovite and biotite. The morphology of this schistosity is spaced and the schistosity domains are represented by tabular and oriented crystals of biotite and the microlithons are mainly composed by quartz and plagioclase, which suggests that this schistosity has been developed by dynamic recrystallization, where pre-kynematic crystals can accumulate enough deformation energy to improve the recrystallization towards the grain boundaries.

Slow uplift, presumably with erosional or tectonic thinning, caused a decrease in pressure with an increase in temperature, which is considered as part of the main episode of the metamorphic evolution, represented by the third deformation (D_3), which produces a series of microfolds in the S_2 and S_3 schistosities, developing a still younger schistosity, S_4. It is represented by the mineral assemblage quartz + sillimanite + biotite + garnet. The microfolds are clearly marked by tabular crystals of biotite. However, folding can be observed in both outcrop and thin section, and small similar and asymmetrical folds, which have been classified as kink folds, define it. S_4 is arranged to aproximately an angle of 30º respect to the main foliation (S_2), developing parallel to the axial axis of kink folds. The strain concentration during the development of this folds produced in some cases a microcracking parallel to the axial and in other cases as kink bands, which let to establish that the undeformed material was anysotropic, with a cizalle strain acting parallel to the main plane of anysotropy defined by the S_2.

A cooling accompanied by an extensive retrograde metamorphism occurred during a late retrograde event.

The relative growth and stability of the minerals during the metamorphic and deformational evolution are recapitulated in TABLE 2.
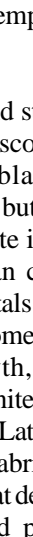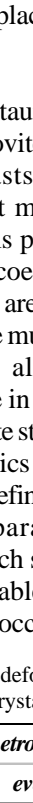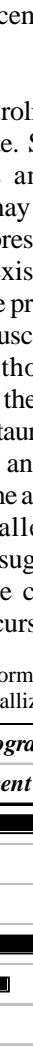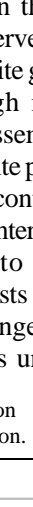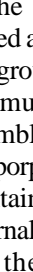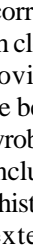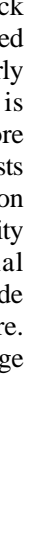
We have observed no clear transition between the fabrics in the high-grade schists and that in the gneiss, so that the age of the gneissic foliation in relation to the deformational history of the schist is uncertain. On the basis of the textural relationships, we consider that it may have formed initially at about the same time as D_2 in the high-grade rocks, but was subsequently modified by compaction or further deformation during partial melting.

Garnet porphyroblasts up to about one centimeter, but more typically about one to three millimetres, in diameter, occurs both the staurolite-kyanite and sillimanite zones and contain inclusions of quartz + ilmenite (± rutile ± muscovite), which commonly define an internal schistosity indicative of early garnet post-kinematic growth. A few micas of S_2 wrap around crystals of garnet (with presure shadows) which are thus pre-tectonic to D_2. Xenoblastic garnet is syntectonic to D_1 and idioblastic garnet is post-tectonic to D_1 or D_2. Pressure shadows are mainly composed of quartz, plagioclase, muscovite and biotite. Garnet porphyroblasts preserve inclusion trails that are discordant to the S_3 external fabric, which are interpreted to record an S_1 fabric deformed during D_1, and suggest deformation by rotation of garnet early during D_2 folding. These garnets may have an inclusion-free rim that separates the core from the discordant external fabric,

and represent the post-D_2 growth. The fabric outside of garnet porphyroblasts generally displays evidence of recrystallization and grain-size coarsening, respect to the inclusion trails in porphyroblasts that occurred during the D_2 phase. The microstructural relationship of small idioblastic matrix garnets that occur in pelitic schists is difficult to interpret, but it is probably that they grew either before or early during D_2. Small inclusion-free garnet grains appear to post-date biotite and muscovite fabric development. According to Castellanos *et al.* (2004), textural sector-zoned garnets from the staurolite-kyanite zone grew in the latest stage of the Silgará Formation metamorphism, during the emplacement of orthogneiss masses.

Porphyroblasts of kyanite and staurolite are concentrated in thin layers of foliated muscovite. Staurolite occurs as nearly euhedral porphyroblasts and commonly has abundant quartz inclusions, but may be, as most grains here, inclusion-free. Staurolite is present in two different textural occurrences that can coexist in the same rock sample. Small staurolite crystals are preserved as corroded relicts in muscovite, so that some muscovite growth clearly post-dated staurolite growth, although muscovite is replaced by fibrolitic sillimanite in the assemblage before final elimination of staurolite. Late staurolite porphyroblasts overgrow the S_2 and/or S_3 fabrics and contain inclusion trails of quartz and ilmenite that define an internal schistosity (S_{int}) continuous with and parallel to the external schistosity (S^{ext} of the rock, which suggests a late episode of heating with an indeterminable change of pressure. However, in some samples, it occurs as unaltered large

TABLE 2. Metamorphic mineral growth from the CSM metamorphic rocks with respect to the deformation history, as well as to the retrograde event. The thicker bars represent more important mineral crystallization.

MINERAL	Tectonic event			Retrograde
PHASES	D_1	D_2	D_3	event
Chlorite				■■■
Ilmenita	■■■■■■■■■■			
Quartz	■■■■■■■■■■■■			
Muscovite	■■■■■■■■■■■■			■■■■
Biotite		■■■■■■■■■■		
Garnet		■■■	■■■	
Staurolite		■■■		
Andalusite		■■■		
Kyanite		■■		
Sillimanite			■■■	
Plagioclase		■■■■■■■■		
K-feldspar			■	

porphyroblasts with an internal foliation defined by straight and, sometimes sigmoidal, inclusion pattern of quartz and ilmenite, which is perpendicular to S_{ext}. Both textural occurrences suggest that staurolite grew inter-kinematically between D_2 and D_2. It appears that staurolite grew some time after garnet in these rocks when they had reached a higher temperature. The kyanite occurs as subidioblastic crystals, although it is commonly observed developing corroded relicts into muscovite. This mineral shows a good cleavage in one direction, as well as partition almost to right angles. It is associated to quartz and, sometimes, staurolite in quartz-rich bands, in which kyanite surrounds staurolite. In micaceous bands kyanite occurs along with muscovite and biotite as large euhedral grains weakly aligned within the mica foliation, whereas it is commonly randomly oriented in quartz-rich domains. Elongate kyanite does not form a mineral lineation but is randomly oriented within foliation planes, suggesting post-kinematic growth. Some reaction rims of muscovite have been developed around kyanite. These reaction rims have nucleate between kyanite and quartz. The kyanite in some cases is replaced by sillimanite, and in other cases is found as relicts in muscovite. On the other hand, the andalusite occurs as euhedral porphyroblasts, with rectangular shape, elongated in the sense of the main foliation and, many of them poikiloblastic, with numerous inclusions of quartz and opaque minerals. Small crystals of kyanite surround some andalusite porphyroblasts.

Sillimanite occurs only in samples from the lower part of the metamorphic sequence. It occurs as fibrolitic bundles generally aligned in the main foliation, although in some rocks it appears randomly oriented. Ríos y García (2001) reported coexisting kyanite and sillimanite in some samples from the transition between the staurolite-kyanite and sillimanite zones. Muscovite occurs in most samples, but is mainly abundant in the upper part of the CSM section, where it defines the regional foliation. In the sillimanite zone a second generation of muscovite appears to overgrow both fibrolite and the regional foliation. Biotite is common to all samples and defines the regional foliation. Staurolite occurs as anhedral grains in the matrix together with kyanite, garnet, biotite, and muscovite. Inger & Harris (1992) also reported staurolite inclusions in garnet from one sample in the sillimanite zone.

Different stages of recrystallization of sillimanite have been recognized, from a fine and felted fibrolite appears to be the sillimanite of earliest formation, to coarse growth of prismatic crystals commonly as stellate aggregates enclosed in biotite. The texture in which coarse sillimanite occurs within biotite may reflect its growth either contemporaneously or subsequent to the recrystallization of the sillimanite. The prismatic sillimanite, in some cases, showing diamond-shape cross sections and good cleavage, develops a strong orientation. A fine fibrolitic sillimanite commonly shows a meandriform aspect through the micaceous bands of the rock, and occurs as intergrowths with, and apparently replacing, biotite. It develops a progressive replacement along the trace of cleavage in biotite, and relicts of biotite within sillimanite are common. The association sillimanite-muscovite also occurs, although there is no regularity of the orientation, because numerous small needle-like crystals of sillimanite traversing muscovite at different angles to the cleavage. Chinner (1961) supposes that if a sillimanite-muscovite texture originally existed, extensive recrystallization and growth of muscovite have destroyed it during the later phases of metamorphism. An acicular variety of sillimanite occurs as minute and isolated crystal across quartz, plagioclase and, less frequently, garnet, as well as along the contact between quartz grains or between quartz and plagioclase grains. The sillimanite also develops pseudomorphs along with biotite and, maybe with leucoxene, replacing garnet, although is possible to think that a previous replacement biotite+muscovite after garnet may occur.

Kyanite is absent in such rocks in which sillimanite is abundant and occurs as coarse-grained prismatic crystals. Some textures involving staurolite, kyanite and muscovite indicate growth of these minerals after the main period of sillimanite development, which shows that the recrystallization of coarse sillimanite has been followed by a retrograde process to staurolite-kyanite zone conditions (Chinner 1961). However, we have no evidences of the occurrence of euhedral kyanite or staurolite within sillimanite, apparently replacing or including it.

In some cases staurolite porphyroblasts, which present numerous quartz inclusions, include relicts of garnet. The recrystallization of muscovite after staurolite or kyanite commonly occurs, and typical textures of this recrystallization are corroded relicts of kyanite or staurolite, and remants of sillimanite, found within muscovite. This growth of muscovite appears to be related to a high activity of water and potassium in the fluid phase at the staurolite-kyanite zone (Chinner 1961).

Muscovite grew during D_1 and D_2, and occurs as strain-free, recrystallized grains around folds. It sometimes occurs as randomly oriented crystals. Muscovite occurs also as a retrograde phase after feldspar, kyanite, garnet and staurolite. Dark brown up to brown redish biotite occur in very different textural positions. It is locally oriented

parallel to S_1, developed during D_1, although it is commonly well oriented parallel to S_2, particularly in the hinge areas of D_2 folds, and grew during D_2. It also occurs as randomly oriented crystals, as inclusions in plagioclase and garnet porphyroblasts or as reaction products of garnet, staurolite and amphibole. Biotite crystals defining S_2 are commonly closely associated or intergrown with sillimanite. All of these textural relationships indicate that biotite was stable during almost the entire metamorphic evolution of these rocks. Alteration of biotite to chlorite has occurred at a very late stage. Chlorite grew during D_1, although this mineral usually occurs as a retrograde phase that partly replaces biotite, garnet and staurolite, developing sometimes pseudomorphs after garnet.

Plagioclase sometimes appears in the matrix as large ovoid porphyroblasts, which show cores densely crowded with inclusions, defining a straight internal foliation or forms inclusion-free rims, as well as new clear porphyroblasts associated with K-feldspar and biotite and/or muscovite.

Ilmenite is the most abundant Fe-Ti oxide in all of the different types of metamorphic rocks. It is present as a matrix component parallel to S_1 or S_2, or as inclusions in garnet and staurolite porphyroblasts. Needle-shaped crystals of ilmenite occur in the three directions within biotite. Rutile is sometimes preserved in large ilmenite crystals, suggesting a texture involving rutile pseudomorphs after ilmenite.

MINERAL CHEMISTRY OF COEXISTING PHASES

Chemical analyses were carried out by an automated JEOL JXA 8800M electron microprobe analyzers from the Geosciences Department at Shimane University, Japan, and the Center of Electron Microscopy at Universidad Complutense de Madrid, Spain, using an accelerating voltage of 15 kV and a beam current of 2.5×10^{-8} A. Data acquisition and reduction were performed using the correction method of Bence & Albee (1968). Natural and synthetic minerals were used as standards. Mineral compositions were determined by multiple spot analyses. Garnet chemical zoning was documented with radial traverses of analytical points (spacing of analytical points decreasing near the rim). The chemical composition of the metamorphic rocks of the Bucaramanga Gneiss, Silgará Formation and Orthogneiss in the CSM show very complex relationships, which reflects a strong control of the chemical compositions of the constituent minerals of these rocks by the bulk-rock chemistry. Representative mineral analyses of the metamorphic rocks are listed in TABLE 3. Mineral abbreviations are after Kretz (1983).

Garnet

Garnet porphyroblasts commonly occur in pelitic and semipelitic rocks of the Silgará Formation and sometimes appear in pelitic rocks of the Bucaramanga Gneiss, but are absent in the Orthogneiss. Representative analyses of garnet are given in TABLE 4. All of the analyzed garnet grains are chemically zoned and rich in almandine in both the Silgará (X_{alm} = 0.60-0.89) and Bucaramanga Gneiss (X_{alm} = 0.60-0.65) formations. The pyrope, grossularie and spessartine contents vary as follows: X_{prp} = 0.18-0.65 (SF) and 0.24-0.37 (BG), X_{grs} = 0.02-0.21 (SF) and 0.05-0.17 (BG), and X_{sps} = 0.00-0.17 (SF) and 0.00-0.17 (BG). Representative profiles were selected from the three different metamorphic zones (FIGURE 3). Chemical zoning can be divided from these zones as follow:

Staurolite-Kyanite Zone, this type of garnets exhibit normal zoning with increasing Mg and Fe components from core to rim and decreasing Mn and Ca component from core to rim, suggesting a prograde stage of metamorphism (sample PCM-971 FIGURE 3).

Lower Sillimanite Zone, this type of garnets exhibit normal zoning through to the inner rim, but in the outer rim the chemical zoning is reverse, reflecting the effects of a retrograde stage of metamorphism. According to the chemical profiles for FeO and MgO, these components increase from core to inner rim, and decrease from inner rim to outer rim, and chemical profile for MnO shows decrease from core to inner rim and increase from inner rim to outer rim (sample PCM-953).

Upper Sillimanite Zone, this type of garnet exhibit normal zoning with a slight increase of FeO, MgO and CaO and decrease of MnO from core to rim, suggesting a prograde stage of high grade of metamorphism evidencing chemical homogenization of components (sample PCM-855).

Staurolite

Staurolite is Fe-rich (X_{Fe} = 0.68-0.89), but does not show any zonation in Fe and Mg. Representative analyses of staurolite are given in TABLE 5. Sample PCM-49 has the ZnO highest content (3.70 weight %) and homogeneous Zn distribution.

Muscovite

Representative muscovite analyses in pelitic rocks of the Silgará Formation are given in TABLE 6. The compositions of muscovite are shown in FIGURE 4, in terms of the

TABLE 3. Representative mineral analyses of the metamorphic rocks in the central Santander Massif. The structural formulae were calculated for garnet, staurolite, muscovite, biotite, plagioclase and amphibole using 8, 23, 22, 22, 8 and 23 oxygens, respectively.

Unit	SF	SF	BG	BG	SF	SF	SF	O	BG	SF	O	BG	SF	O	BG
Met. zone	St-Ky	St-Ky	Sil	Sil	St-Ky	St-Ky	St-Ky	St-Ky	Sil	St-Ky	St-Ky	Sil	St-Ky	St-Ky	Sil
Sample No.	PCM-16	PCM-28	PCM-156	PCM-855	PCM-16	PCM-16	PCM-16	PCM-638	PCM-855	PCM-28	PCM-638	PCM-855	PCM-28	PCM-638	PCM-855
Mineral	Grt	Grt	Grt	Grt	St	Ms	Bt	Bt	Bt	Pl	Pl	Pl	Fe-Ts	Mg-Hbl	Ts
SiO_2	36.90	37.74	37.82	38.15	27.80	45.12	35.02	37.13	35.92	59.31	52.91	56.60	40.72	47.59	42.10
TiO_2	0.01	0.06	0.00	0.00	0.64	0.42	2.30	3.07	2.73	0.00	0.00	0.00	0.39	0.55	0.60
Al_2O_3	22.16	22.25	21.90	21.80	55.16	37.60	20.22	15.66	16.20	26.19	29.85	27.30	18.11	10.27	12.93
Fe_2O_3	0.00	0.00	0.00	0.00	0.00	0.00	0.00	0.00	0.00	0.00	0.00	0.00	4.18	1.16	15.04
FeO	35.26	28.78	28.04	26.56	13.46	0.82	19.91	12.80	17.50	0.02	0.09	0.16	13.67	9.50	4.27
MnO	1.81	1.57	7.36	4.51	0.11	0.05	0.07	0.13	0.20	0.02	0.01	0.00	0.22	0.15	0.81
MgO	3.17	3.20	3.05	3.52	1.22	0.59	8.55	15.11	12.91	0.01	0.00	0.00	6.76	14.07	10.60
CaO	0.51	6.66	1.77	5.49	0.01	0.03	0.01	0.02	0.03	7.72	12.40	9.10	11.61	12.53	10.20
Na_2O	0.00	0.00	0.00	0.00	0.00	1.26	0.42	0.36	0.27	7.00	4.56	6.50	1.05	0.94	1.40
K_2O	0.00	0.00	0.00	0.00	0.00	9.47	8.80	8.80	9.41	0.07	0.06	0.08	0.43	0.55	0.40
Cr_2O_3	0.00	0.00	0.02	0.00	0.00	0.00	0.00	0.03	0.02	0.00	0.00	0.00	0.06	0.06	0.00
Total	99.82	100.26	99.96	100.03	98.40	95.36	95.33	93.08	95.19	100.34	99.88	99.74	97.20	97.37	98.35
Si	2.97	2.98	3.02	3.01	3.82	5.97	5.32	5.60	5.45	2.64	2.40	2.55	6.07	6.87	6.14
Ti	0.00	0.00	0.00	0.00	0.07	0.04	0.26	0.35	0.31	0.00	0.00	0.00	0.04	0.06	0.07
Al	2.10	2.07	2.06	2.03	8.94	5.86	3.62	2.78	2.90	1.37	1.60	1.45	3.18	1.75	2.22
Fe^{3+}	0.00	0.00	0.00	0.00	0.00	0.00	0.00	0.00	0.00	0.00	0.00	0.00	0.47	0.13	1.71
Fe^{2+}	2.37	1.90	1.87	1.75	1.55	0.09	2.53	1.61	2.22	0.00	0.00	0.01	1.72	1.15	0.54
Mn	0.12	0.11	0.50	0.30	0.01	0.01	0.01	0.02	0.03	0.00	0.00	0.00	0.03	0.02	0.10
Mg	0.38	0.38	0.36	0.41	0.25	0.12	1.94	3.40	2.92	0.00	0.00	0.00	1.50	3.03	2.30
Ca	0.04	0.56	0.15	0.46	0.00	0.00	0.00	0.00	0.01	0.37	0.60	0.44	1.85	1.94	1.59
Na	0.00	0.00	0.00	0.00	0.00	0.32	0.12	0.11	0.08	0.60	0.40	0.57	0.30	0.26	0.40
K	0.00	0.00	0.00	0.00	0.00	1.60	1.71	1.69	1.82	0.00	0.00	0.01	0.08	0.10	0.07
Cr	0.00	0.00	0.00	0.00	0.00	0.00	0.00	0.00	0.00	0.00	0.00	0.00	0.01	0.01	0.00
Total	7.98	7.99	7.96	7.97	14.64	14.02	15.52	15.56	15.74	4.98	5.01	5.01	15.27	15.31	15.15
X_{Fe}	0.86	0.83	0.84	0.81	0.86		0.57	0.32	0.43				0.53	0.28	0.19
X_{alm}	0.81	0.65	0.65	0.60											
X_{sps}	0.04	0.04	0.17	0.10											
X_{prp}	0.57	0.33	0.24	0.28											
X_{grs}	0.02	0.19	0.05	0.16											
X_{An}										0.38	0.60	0.43			

*Total Fe as $FeO+Fe_2O_3$. Fe^{3+} from stoichiometry according to Leake et al. (1997).

$X_{Fe} = Fe^{2+}/(Fe^{2+}+Mg)$, $X_{alm} = Fe^{2+}/(Fe^{2+}+Mn+Mg+Ca)$, $X_{sps} = Mn/(Fe^{2+}+Mn+Mg+Ca)$, $X_{prp} = Mg/(Fe^{2+}+Mn+Mg+Ca)$, $X_{grs} = Ca/(Fe^{2+}+Mn+Mg+Ca)$. $X_{An} = Ca/(Na+Ca+K)$.

BG = Bucaramanga Gneiss, SF = Silgará Formation, O = Orthogneiss. Mineral abreviations after Kretz (1983).

TABLE 4. Representative chemical compositions of garnet from metapelitic rocks of the Silgará Formation in the central Santander Massif. PS: Pelitic Schists.

| Lithology	PS	PS	PS	PS	PS	PS	PS	PS	PS	PS	PS	PS	PS	PS	PS	PS	PS	PS
Sample No.	PCM-47		PCM-618		PCM-651		PCM-700		PCM-701		PCM-702		PCM-953			PCM-971		
Analysis No.	3	12	5SZ	6SZ	14	13	1	7	9	16	1	7	1	18	23	4	5	6
Weight %	mantle	rim	rim	core	core	rim	core	rim	core	rim	core	rim	core	mantle	rim	rim	mantle	core
SiO_2	36.44	37.10	36.84	36.58	37.74	37.51	36.07	36.10	36.68	36.51	36.70	37.06	37.31	37.28	37.28	37.03	36.99	36.41
TiO_2	0.14	0.02	0.00	0.01	0.04	0.02	0.02	0.04	0.03	0.04	0.00	0.00	0.00	0.02	0.00	0.00	0.00	0.00
Al_2O_3	20.23	20.57	20.68	20.62	21.01	21.11	19.95	20.16	20.36	20.45	20.46	20.73	21.03	21.08	21.07	21.04	20.72	20.29
FeO*	33.69	35.66	34.75	35.23	34.29	34.72	41.06	41.55	38.08	38.83	37.09	39.13	31.24	34.67	30.89	35.41	35.13	33.53
MnO	4.04	1.49	0.10	0.99	1.07	0.16	0.03	0.02	0.88	0.31	1.62	0.19	6.07	2.46	6.95	0.14	2.45	4.38
MgO	1.88	3.06	2.69	1.76	2.69	3.01	1.37	1.39	1.57	1.82	1.72	2.49	1.96	3.05	2.60	3.75	2.15	1.39
CaO	3.46	2.66	3.31	3.59	4.09	3.35	0.37	0.31	1.58	1.09	1.62	0.77	2.97	1.99	1.73	2.21	2.32	2.80
Na_2O	0.01	0.01	0.04	0.00	0.00	0.02	0.07	0.01	0.01	0.09	0.00	0.05	0.11	0.00	0.07	0.03	0.00	0.04
K_2O	0.01	0.05	0.01	0.03	0.03	0.05	0.01	0.05	0.05	0.04	0.04	0.05	0.04	0.02	0.03	0.03	0.02	0.05
Cr_2O_3	0.00	0.00	0.01	0.02	0.03	0.01	0.01	0.00	0.00	0.00	0.01	0.02	0.01	0.00	0.00	0.04	0.01	0.01
Total	99.90	100.60	98.44	98.82	100.99	99.95	98.96	99.63	99.24	99.15	99.25	100.48	100.74	100.58	100.62	99.67	99.78	98.89
Cations per 12 O																		
Si	2.975	2.987	3.009	2.998	3.006	3.008	3.000	2.987	3.015	3.004	3.011	3.001	3.002	2.990	2.997	2.983	3.004	3.003
Ti	0.009	0.001	0.000	0.001	0.003	0.001	0.001	0.002	0.002	0.002	0.000	0.000	0.000	0.001	0.000	0.000	0.000	0.000
Al	1.947	1.951	1.990	1.992	1.971	1.995	1.956	1.965	1.972	1.983	1.979	1.979	1.993	1.992	1.997	1.997	1.984	1.972
Fe^{3+}	0.085	0.074	0.000	0.011	0.012	0.000	0.041	0.057	0.000	0.004	0.000	0.020	0.003	0.025	0.008	0.038	0.008	0.023
Fe^{2+}	2.216	2.326	2.373	2.403	2.272	2.329	2.815	2.818	2.617	2.668	2.545	2.629	2.098	2.300	2.069	2.347	2.378	2.290
Mn	0.279	0.102	0.007	0.069	0.072	0.011	0.002	0.001	0.061	0.022	0.112	0.013	0.414	0.167	0.473	0.010	0.168	0.306
Mg	0.229	0.367	0.327	0.215	0.319	0.360	0.170	0.171	0.192	0.223	0.210	0.301	0.235	0.365	0.311	0.450	0.260	0.171
Ca	0.303	0.229	0.290	0.315	0.349	0.287	0.033	0.027	0.139	0.096	0.142	0.066	0.256	0.171	0.149	0.190	0.202	0.247
Na	0.004	0.003	0.014	0.000	0.000	0.005	0.023	0.004	0.002	0.029	0.001	0.015	0.036	0.000	0.021	0.009	0.000	0.013
K	0.003	0.010	0.003	0.006	0.007	0.010	0.003	0.011	0.010	0.009	0.009	0.011	0.009	0.004	0.006	0.007	0.005	0.010
Cr	0.000	0.000	0.001	0.001	0.002	0.001	0.001	0.000	0.000	0.000	0.000	0.001	0.000	0.000	0.000	0.003	0.001	0.000
Total	8.049	8.050	8.013	8.011	8.012	8.007	8.046	8.044	8.010	8.039	8.009	8.036	8.046	8.017	8.032	8.034	8.008	8.035
*Total Fe as FeO + Fe_2O_3																		
Numbers of ions on the basis of 12 O																		
Si	2.975	2.987	3.009	2.998	3.006	3.008	3.000	2.987	3.015	3.004	3.011	3.001	3.002	2.990	2.997	2.983	3.004	3.003
Al^{IV}	0.025	0.013	0.000	0.002	0.000	0.000	0.000	0.013	0.000	0.000	0.000	0.000	0.000	0.010	0.003	0.017	0.000	0.000
sum T	3.000	3.000	3.009	3.000	3.006	3.008	3.000	3.000	3.015	3.004	3.011	3.001	3.002	3.000	3.000	3.000	3.004	3.003
Al^{VI}	1.922	1.938	1.990	1.990	1.971	1.995	1.956	1.952	1.972	1.983	1.979	1.979	1.993	1.982	1.994	1.980	1.984	1.972
Cr	0.000	0.000	0.001	0.001	0.002	0.001	0.001	0.000	0.000	0.000	0.000	0.001	0.000	0.000	0.000	0.003	0.001	0.000
Fe^{3+}	0.085	0.074	0.000	0.011	0.012	0.000	0.041	0.057	0.000	0.004	0.000	0.020	0.003	0.025	0.008	0.038	0.008	0.023
Ti	0.009	0.001	0.000	0.001	0.003	0.001	0.001	0.002	0.002	0.002	0.000	0.000	0.000	0.001	0.000	0.000	0.000	0.000
sum Y	2.016	2.012	1.991	2.003	1.987	1.997	1.999	2.011	1.974	1.989	1.979	2.000	1.997	2.009	2.003	2.020	1.992	1.995
Mg	0.229	0.367	0.327	0.215	0.319	0.360	0.170	0.171	0.192	0.223	0.210	0.301	0.235	0.365	0.311	0.450	0.260	0.171
Fe^{2+}	2.216	2.326	2.373	2.403	2.272	2.329	2.815	2.818	2.617	2.668	2.545	2.629	2.098	2.300	2.069	2.347	2.378	2.290
Mn	0.279	0.102	0.007	0.069	0.072	0.011	0.002	0.001	0.061	0.022	0.112	0.013	0.414	0.167	0.473	0.010	0.168	0.306
Ca	0.303	0.229	0.290	0.315	0.349	0.287	0.033	0.027	0.139	0.096	0.142	0.066	0.256	0.171	0.149	0.190	0.202	0.247
sum X	3.026	3.025	2.996	3.002	3.012	2.987	3.021	3.018	3.010	3.009	3.009	3.009	3.003	3.004	3.002	2.998	3.008	3.014
Total	8.042	8.037	7.996	8.005	8.005	7.993	8.020	8.029	7.998	8.002	7.999	8.010	8.001	8.013	8.004	8.018	8.004	8.011
X_{Mg}	0.09	0.14	0.12	0.08	0.12	0.13	0.06	0.06	0.07	0.08	0.08	0.10	0.10	0.14	0.13	0.16	0.10	0.07
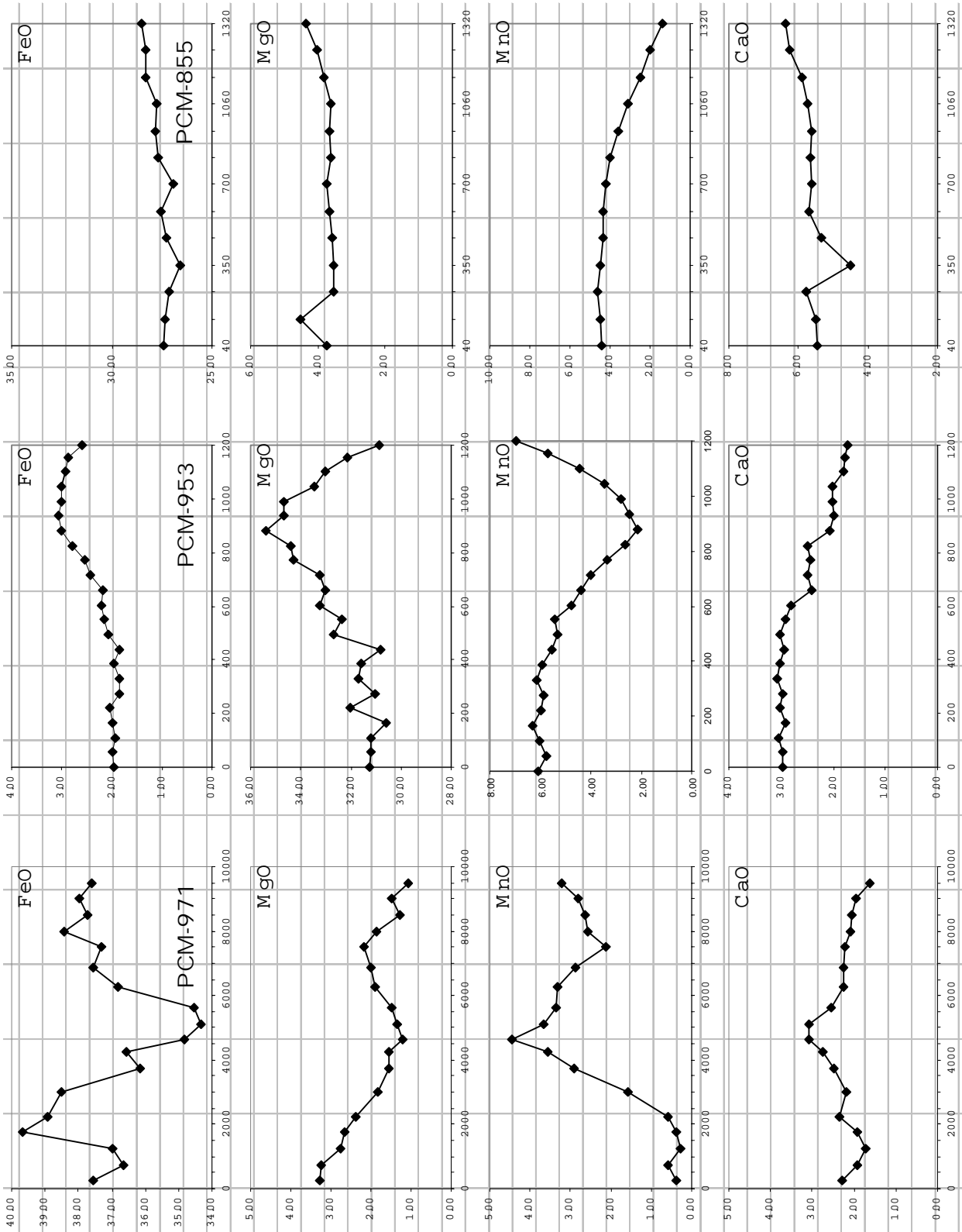
FIGURE 3. Chemical profiles for pelitic garnet in samples PCM-971, PCM-953, and PCM-855 from metamorphic rocks in the central Santander Massif.

TABLE 5. Representative chemical compositions of staurolite from metapelitic rocks of the Silgará Formation in the central Santander Massif. PS: Pelitic Schists.

Lithology	PS	PS	PS	PS	PS	PS	PS	PS	PS	PS	PS	PS	PS
Sample No.	PCM-20	PCM-21	PCM-47	PCM-49	PCM-618	PCM-651	PCM-700	PCM-701	PCM-702	PCM-905	PCM-907	PCM-940	PCM-971
Analysis No.	8	1	7	3	4	8	2	18	8	7	4	5	4
Weight %													
SiO_2	26.95	27.94	27.86	27.74	26.55	27.56	26.44	26.97	28.62	27.31	27.11	26.54	26.68
TiO_2	0.46	0.46	0.52	0.40	0.52	0.63	0.64	0.70	0.55	0.58	0.52	0.81	0.60
Al_2O_3	54.44	52.81	53.17	52.77	54.48	52.68	53.64	53.78	51.85	52.97	53.33	53.76	53.17
FeO*	13.43	12.79	13.80	9.22	13.19	14.50	13.94	14.76	14.97	13.79	13.84	13.16	14.05
MnO	0.02	0.50	0.06	1.24	0.01	0.05	0.01	0.03	0.03	0.29	0.41	0.64	0.15
MgO	2.42	2.27	1.81	2.39	1.21	1.55	0.92	1.52	1.45	1.94	1.89	1.54	1.28
CaO	0.03	0.00	0.00	0.02	0.00	0.00	0.00	0.00	0.02	0.02	0.00	0.01	0.00
Na_2O	0.02	0.00	0.02	0.14	0.08	0.01	0.01	0.00	0.00	0.03	0.00	0.07	0.07
K_2O	0.01	0.03	0.03	0.03	0.04	0.02	0.01	0.06	0.03	0.03	0.03	0.06	0.04
ZnO	0.08	0.61	0.15	3.70	1.34	0.50	0.62	0.05	0.12	0.05	0.30	1.16	1.36
Cr_2O_3	0.01	0.04	0.04	0.03	0.04	0.08	0.04	0.05	0.05	0.06	0.04	0.05	0.00
Total	97.87	97.44	97.44	97.67	97.47	97.58	96.27	97.92	97.67	97.07	97.47	97.81	97.39
Cations per 23 oxygens													
Si	3.738	3.896	3.884	3.876	3.720	3.862	3.748	3.763	3.999	3.831	3.795	3.717	3.761
Ti	0.048	0.048	0.054	0.042	0.055	0.066	0.069	0.073	0.057	0.061	0.055	0.086	0.064
Al	8.900	8.679	8.737	8.689	8.995	8.699	8.963	8.844	8.539	8.757	8.797	8.873	8.835
Fe^{3+}	0.000	0.000	0.000	0.000	0.000	0.000	0.000	0.000	0.000	0.000	0.000	0.000	0.000
Fe^{2+}	1.558	1.491	1.609	1.077	1.545	1.698	1.653	1.722	1.749	1.617	1.620	1.542	1.657
Mn	0.002	0.059	0.006	0.146	0.001	0.005	0.001	0.004	0.003	0.035	0.048	0.076	0.017
Mg	0.500	0.471	0.377	0.498	0.253	0.325	0.194	0.316	0.301	0.406	0.394	0.322	0.268
Ca	0.004	0.000	0.000	0.003	0.001	0.000	0.000	0.000	0.003	0.003	0.000	0.001	0.000
Na	0.005	0.000	0.005	0.039	0.021	0.002	0.003	0.000	0.000	0.008	0.001	0.019	0.019
K	0.002	0.005	0.005	0.005	0.007	0.004	0.001	0.011	0.005	0.005	0.005	0.011	0.007
Zn	0.008	0.062	0.015	0.382	0.139	0.051	0.065	0.005	0.012	0.005	0.031	0.120	0.141
Cr	0.001	0.005	0.005	0.003	0.004	0.009	0.005	0.006	0.005	0.006	0.005	0.006	0.000
Total	14.767	14.717	14.696	14.759	14.740	14.722	14.702	14.744	14.674	14.733	14.752	14.772	14.771
*Total Fe as FeO													
Numbers of ions on the basis of 23 O													
Si	3.738	3.896	3.884	3.876	3.720	3.862	3.748	3.763	3.999	3.831	3.795	3.717	3.761
Al^{IV}	0.262	0.104	0.116	0.124	0.280	0.138	0.252	0.237	0.001	0.169	0.205	0.283	0.239
sum T	4.000	4.000	4.000	4.000	4.000	4.000	4.000	4.000	4.000	4.000	4.000	4.000	4.000
Al^{VI}	8.638	8.575	8.620	8.565	8.715	8.561	8.711	8.607	8.538	8.587	8.593	8.591	8.596
Cr	0.001	0.005	0.005	0.003	0.004	0.009	0.005	0.006	0.005	0.006	0.005	0.006	0.000
Ti	0.048	0.048	0.054	0.042	0.055	0.066	0.069	0.073	0.057	0.061	0.055	0.086	0.064
Fe^{2+}	1.558	1.491	1.609	1.077	1.545	1.698	1.653	1.722	1.749	1.617	1.620	1.542	1.657
Mn	0.002	0.059	0.006	0.146	0.001	0.005	0.001	0.004	0.003	0.035	0.048	0.076	0.017
Zn	0.008	0.062	0.015	0.382	0.139	0.051	0.065	0.005	0.012	0.005	0.031	0.120	0.141
Mg	0.500	0.471	0.377	0.498	0.253	0.325	0.194	0.316	0.301	0.406	0.394	0.322	0.268
sum Y	10.756	10.712	10.687	10.712	10.712	10.715	10.698	10.733	10.666	10.718	10.746	10.741	10.744
Ca	0.004	0.000	0.000	0.003	0.001	0.000	0.000	0.000	0.003	0.003	0.000	0.001	0.000
Na	0.005	0.000	0.005	0.039	0.021	0.002	0.003	0.000	0.000	0.008	0.001	0.019	0.019
K	0.002	0.005	0.005	0.005	0.007	0.004	0.001	0.011	0.005	0.005	0.005	0.011	0.007
sum X	0.012	0.005	0.009	0.047	0.028	0.006	0.004	0.011	0.008	0.015	0.006	0.031	0.027
Total	14.767	14.716	14.696	14.759	14.740	14.721	14.702	14.744	14.674	14.733	14.752	14.772	14.771
X_{Mg}	0.24	0.24	0.19	0.32	0.14	0.16	0.11	0.16	0.15	0.20	0.20	0.17	0.14

TABLE 6. Representative chemical compositions of muscovite from metapelitic rocks of the Silgará Formation in the central Santander Massif. PS: Pelitic Schists. inc.Bt: inclusion in biotite; inc.Grt: inclusion in garnet; M: matrix.

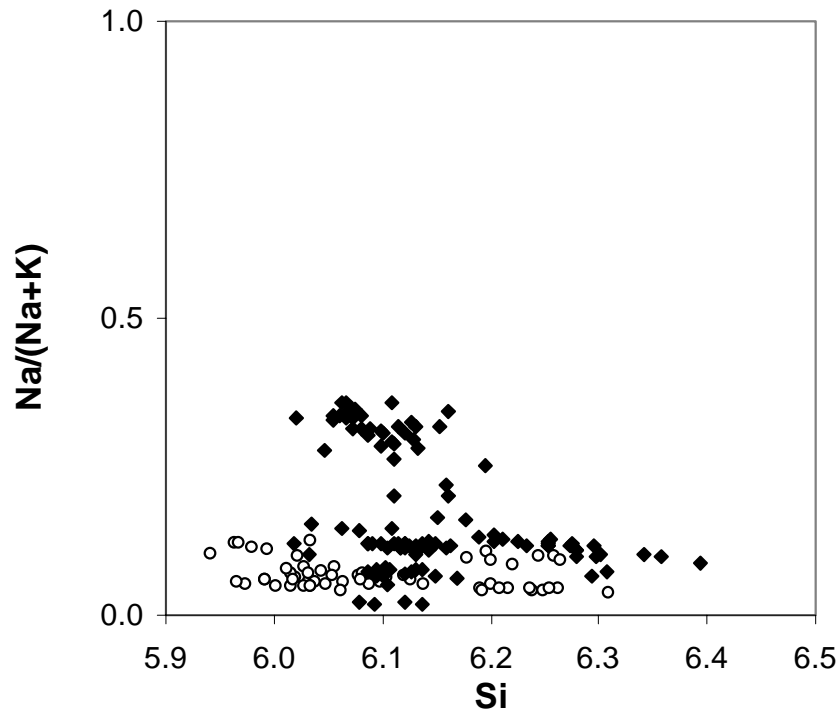| Lithology	PS	PS	PS	PS	PS	PS	PS	PS	PS	PS	PS	PS	PS	PS	PS	PS	PS	PS	PS	PS
Sample No.	PCM-18	PCM-24	PCM-21	PCM-47	PCM-49	PCM-416	PCM-418	PCM-651	PCM-706	PCM-T61	PCM-782	PCM-685	PCM-893	PCM-894	PCM-897	PCM-940	PCM-963	PCM-671	PCM-972	PCM-881
Analysis No.	7	1	4	4	6	1	7	2	2	8	5	3	3	4	4	4	7	3	4	6
	inc. Bt	M	M	M	M	M	M	M	M	M	M	M	M	M	M	M	M	inc. Grt	M	M
Weight %																				
SiO_2	45.09	45.77	47.41	45.43	47.81	45.69	47.69	45.22	45.46	45.07	45.23	45.36	44.91	46.34	44.61	45.43	45.11	44.76	44.14	43.77
TiO_2	0.58	0.23	0.37	0.32	0.31	0.65	0.70	0.79	0.22	0.37	0.39	0.43	0.68	0.96	0.92	0.92	1.00	0.48	0.87	0.83
Al_2O_3	34.66	35.34	34.29	35.09	33.01	34.77	35.82	34.80	35.87	36.00	35.69	32.07	35.92	35.74	34.05	36.40	34.09	35.56	35.03	35.01
FeO^*	2.95	2.43	2.98	0.75	2.77	3.42	1.96	1.17	0.88	0.55	0.81	4.05	1.13	1.65	2.34	1.26	1.59	1.92	1.48	1.50
MnO	0.04	0.00	0.01	0.02	0.01	0.01	0.00	0.01	0.04	0.00	0.02	0.00	0.00	0.01	0.06	0.00	0.04	0.04	0.00	0.00
MgO	0.71	0.57	0.97	0.49	0.92	1.12	0.58	0.62	0.23	0.17	0.33	0.59	0.58	0.02	0.71	0.81	0.72	0.50	0.68	0.67
CaO	0.00	0.00	0.00	0.01	0.03	0.04	0.00	0.00	0.01	0.02	0.03	0.02	0.00	0.00	0.02	0.03	0.00	0.00	0.04	0.03
Na_2O	1.17	2.36	0.91	1.54	0.57	0.16	0.82	0.86	2.31	2.39	2.25	0.31	0.57	0.49	0.43	0.42	0.96	0.64	0.75	0.52
K_2O	10.33	7.49	9.31	9.28	9.06	10.23	9.34	10.42	8.30	8.09	8.29	10.52	10.04	10.82	10.18	10.58	10.60	9.83	10.40	10.24
Cr_2O_3	0.00	0.02	0.02	0.07	0.01	0.00	0.03	0.00	0.07	0.06	0.05	0.00	0.04	0.00	0.01	0.03	0.03	0.03	0.06	0.03
Total	95.53	94.22	96.27	92.99	94.50	95.60	96.05	93.89	93.20	52.71	93.09	93.35	93.87	96.82	93.33	95.87	94.13	93.76	93.44	92.59
Cations per 22 Oxygens																				
Si	6.064	6.127	6.254	6.160	6.384	6.122	6.234	6.121	6.129	6.098	6.109	6.262	6.656	6.095	6.104	6.019	6.120	6.064	6.023	6.017
Ti	0.059	0.023	0.036	0.033	0.031	0.066	0.069	0.080	0.022	0.038	0.040	0.045	0.069	0.095	0.095	0.091	0.102	0.049	0.089	0.086
Al	5.493	5.576	5.330	5.608	5.262	5.411	5.518	5.551	5.696	5.739	5.680	5.218	5.708	5.539	5.489	5.683	5.451	5.677	5.632	5.673
Fe^{3+}	0.331	0.272	0.328	0.085	0.310	0.384	0.116	0.133	0.076	0.063	0.091	0.468	0.128	0.182	0.267	0.139	0.181	0.217	0.169	0.173
Mn	0.005	0.000	0.001	0.002	0.001	0.001	0.000	0.001	0.005	0.000	0.003	0.000	0.000	0.001	0.007	0.000	0.004	0.004	0.000	0.000
Mg	0.141	0.113	0.191	0.098	0.184	0.224	0.113	0.125	0.047	0.034	0.066	0.121	0.116	0.161	0.145	0.159	0.146	0.101	0.139	0.138
Ca	0.000	0.000	0.000	0.001	0.005	0.006	0.000	0.000	0.001	0.003	0.004	0.003	0.000	0.000	0.002	0.004	0.000	0.000	0.006	0.004
Na	0.306	0.613	0.232	0.404	0.147	0.041	0.209	0.226	0.602	0.628	0.590	0.083	0.149	0.126	0.115	0.108	0.251	0.168	0.197	0.137
K	1.771	1.279	1.567	1.606	1.545	1.748	1.557	1.799	1.426	1.396	1.429	1.852	1.727	1.814	1.776	1.788	1.835	1.699	1.811	1.795
Cr	0.000	0.002	0.003	0.007	0.001	0.000	0.003	0.000	0.008	0.006	0.005	0.000	0.005	0.000	0.001	0.003	0.003	0.003	0.006	0.003
Total	14.170	14.006	13.943	14.004	13.820	14.002	13.819	14.036	14.012	14.004	14.018	14.052	13.557	14.012	14.002	13.995	14.053	13.982	14.073	14.026
*Total Fe as FeO																				
Numbers of ions on the basis of 22 O																				
Si	6.064	6.127	6.254	6.160	6.384	6.122	6.234	6.121	6.129	6.098	6.109	6.262	6.656	6.095	6.104	6.019	6.120	6.064	6.023	6.017
Al^{IV}	1.936	1.873	1.746	1.840	1.606	1.878	1.766	1.879	1.871	1.902	1.891	1.738	1.344	1.905	1.896	1.981	1.880	1.936	1.977	1.983
sum T	8.000	8.000	8.000	8.000	8.000	8.000	8.000	8.000	8.000	8.000	8.000	8.000	8.000	8.000	8.000	8.000	8.000	8.000	8.000	8.000
Al^{VI}	3.556	3.703	3.584	3.768	3.596	3.532	3.752	3.672	3.825	3.837	3.789	3.480	3.764	3.633	3.593	3.702	3.571	3.741	3.656	3.690
Cr	0.000	0.002	0.003	0.007	0.001	0.000	0.003	0.000	0.008	0.006	0.005	0.003	0.005	0.000	0.001	0.003	0.003	0.003	0.006	0.003
Ti	0.059	0.023	0.036	0.033	0.031	0.066	0.069	0.080	0.022	0.038	0.040	0.045	0.069	0.095	0.095	0.091	0.102	0.049	0.089	0.086
Fe^{2+}	0.331	0.272	0.328	0.085	0.310	0.224	0.116	0.133	0.076	0.063	0.091	0.468	0.128	0.182	0.267	0.139	0.181	0.217	0.169	0.173
Mn	0.005	0.000	0.001	0.002	0.001	0.001	0.000	0.001	0.005	0.000	0.003	0.000	0.000	0.001	0.007	0.000	0.004	0.004	0.000	0.000
Mg	0.141	0.113	0.191	0.098	0.184	0.224	0.113	0.125	0.047	0.034	0.066	0.121	0.116	0.161	0.145	0.159	0.146	0.101	0.139	0.138
sum Y	4.093	4.115	4.143	3.993	4.122	4.207	4.054	4.011	3.982	3.977	3.995	4.114	4.081	4.071	4.108	4.095	4.007	4.114	4.059	4.089
Ca	0.000	0.000	0.000	0.001	0.005	0.006	0.000	0.000	0.001	0.003	0.004	0.003	0.000	0.000	0.002	0.004	0.000	0.000	0.006	0.004
Na	0.306	0.613	0.232	0.404	0.147	0.041	0.209	0.226	0.602	0.628	0.590	0.083	0.149	0.126	0.115	0.108	0.251	0.168	0.197	0.137
K	1.771	1.279	1.567	1.606	1.545	1.748	1.557	1.799	1.426	1.396	1.429	1.852	1.727	1.814	1.776	1.788	1.835	1.699	1.811	1.795
sum X	2.077	1.891	1.799	2.011	1.697	1.795	1.746	2.025	2.029	2.027	2.023	1.938	1.876	1.940	1.893	1.899	2.086	1.867	2.014	1.937
Total	14.169	14.006	13.943	14.004	13.820	14.002	13.819	14.036	14.012	14.004	14.018	14.051	13.557	14.011	14.002	13.995	14.053	13.982	14.073	14.026
X_{Si}	0.03	0.06	0.13	0.08	0.20	0.06	0.12	0.06	0.06	0.05	0.05	0.13	0.03	0.05	0.05	0.01	0.06	0.03	0.01	0.01
Na/(Na+K)	0.15	0.32	0.13	0.20	0.09	0.02	0.12	0.11	0.30	0.31	0.29	0.04	0.08	0.06	0.06	0.06	0.12	0.09	0.10	0.07

FIGURE 4. Chemical composition of the muscovite for pelitic schists from the Silgará Formation in the Mutiscua area, central Santander Massif. Open circles indicate muscovite from the lower sillimanite zone; black rombs indicate muscovite from the staurolite-kyanite zone.

celadonite content, $X_{Si}=(Si/2)-3$, and the paragonite/muscovite ratio. It is possible to difference two groups represented by open circles and black rombs, which could be related to muscovites with different sizes of grain.

For the Staurolite-Kyanite zone Si content ranges from 6.025 to 6.400 and the Na/(Na+K) ratio varies from 0.01 to 0.425. For the Lower Sillimanite Zone, Si content ranges from 5.940 to 6.310 and the Na/(Na+K) ratio varies from 0.045 to 0.092.

The mole fraction of paragonite decreases with increasing celadonite component, and increases with increasing metamorphic grade (temperature) for a fixed celadonite component.

Biotite

Representative biotite analyses are given in TABLE 7. TiO_2 content in biotite ranges from 0.93 to 3.31, which shows a positive correlation with metamorphic grade. $X_{Mg} = 0.21$-0.76. Al^{IV} varies from 2.273 to 2.833, and Al^{VI} varies from 0.552 to 0.913, indicating slight solid solution towards dioctahedral micas (FIGURE 5).

Plagioclase

The anorthite content of plagioclase (X_{An}) varies from 0.03 to 0.61, which increases with the grade of metamorphism. Representative analyses of plagioclase are given in TABLE 8. A ternary diagram illustrates the chemical composition of plagioclase (FIGURE 6).

METAMORPHIC EVOLUTION OF CSM

We have interpreted the conditions of metamorphism using metamorphic pressure and temperature estimates and reaction history to evaluate the P-T path along which the metamorphic rocks in the CSM have been tectonically transported.

Quantitative P-T determinations

P-T conditions of metamorphism have been estimated from metamorphic rocks of the CSM by Berman´s TWQ program and range from 5.0 to 9.5 kbar and from 630 to 727°C. The results of P-T calculations are summarized in TABLE 9.

Metamorphic temperatures were estimated using Fe-Mg partitioning between coexisting garnet and biotite by different calibrations as shown in TABLE 9. The higher

TABLE 7. Representative chemical compositions of biotite from metapelitic rocks of the Silgará Formation in the central Santander Massif. PS: Pelitic Schists. M: matrix.

| Lithology	PS	PS	PS	PS	PS	PS	PS	PS	PS	PS	PS	PS	PS	PS	PS	PS	PS
Sample No.	PCM-18	PCM-20	PCM-21	PCM-28	PCM-49	PCM-610	PCM-618	PCM-651	PCM-885	PCM-893	PCM-894	PCM-897	PCM-940	PCM-953	PCM-971	PCM-972	PCM-981
Analysis No.	1	1	1	1	1	2	10	1	1	1	1	1	1	1	4	1	1
Weight %	M	M	M	M	M	M	M	M	M	M	M	M	M	M	M	M	M
SiO_2	36.95	36.98	36.57	35.70	39.67	38.20	35.00	34.92	33.10	33.85	34.77	34.19	34.84	34.74	34.29	33.61	34.19
TiO_2	1.08	1.37	1.24	1.41	0.93	0.96	2.51	2.08	1.95	2.91	2.88	3.08	3.01	3.07	2.71	2.98	3.31
Al_2O_3	18.92	18.19	19.48	18.56	18.73	20.49	18.63	19.35	17.81	19.61	18.94	18.05	19.75	19.40	19.25	19.62	20.03
FeO*	10.78	14.75	15.16	18.35	11.84	10.52	20.73	20.19	27.57	21.05	18.65	22.45	20.01	19.57	21.17	21.30	21.27
MnO	0.40	0.02	0.18	0.00	0.27	0.16	0.01	0.03	0.23	0.19	0.31	0.31	0.22	0.30	0.11	0.31	0.28
MgO	16.79	14.04	13.21	11.91	15.26	18.55	8.09	9.33	4.21	7.87	9.20	7.93	8.62	8.16	7.22	7.98	7.73
CaO	0.04	0.00	0.01	0.01	0.06	0.08	0.00	0.01	0.00	0.02	0.01	0.00	0.00	0.00	0.00	0.04	0.02
Na_2O	0.47	0.57	0.41	0.47	0.37	0.13	0.46	0.38	0.17	0.40	0.36	0.49	0.39	0.34	0.35	0.42	0.43
K_2O	8.75	9.15	8.36	8.86	8.18	6.67	8.95	9.39	9.75	9.53	10.25	10.08	9.67	9.61	9.19	9.71	9.82
Cr_2O_3	0.04	0.01	0.00	0.02	0.03	0.00	0.00	0.03	0.02	0.06	0.00	0.00	0.02	0.04	0.01	0.06	0.03
Total	94.20	95.07	94.61	95.30	95.33	95.74	94.38	95.71	94.79	95.48	95.36	96.57	96.52	95.23	94.29	96.04	97.07
Cations per 22 O																	
Si	5.438	5.502	5.447	5.395	5.727	5.418	5.412	5.321	5.334	5.215	5.319	5.271	5.270	5.319	5.334	5.167	5.187
Ti	0.119	0.153	0.138	0.160	0.101	0.102	0.292	0.238	0.236	0.337	0.332	0.357	0.342	0.354	0.317	0.345	0.377
Al	3.282	3.190	3.420	3.306	3.187	3.425	3.396	3.474	3.383	3.562	3.414	3.280	3.520	3.501	3.528	3.556	3.581
Fe^{2+}	1.327	1.835	1.888	2.319	1.429	1.248	2.680	2.572	3.715	2.712	2.385	2.895	2.531	2.505	2.753	2.739	2.698
Mn	0.049	0.003	0.023	0.000	0.033	0.019	0.001	0.004	0.031	0.024	0.040	0.040	0.028	0.039	0.014	0.040	0.035
Mg	3.684	3.115	2.933	2.683	3.284	3.922	1.866	2.119	1.010	1.807	2.097	1.823	1.943	1.862	1.674	1.830	1.747
Ca	0.007	0.000	0.001	0.001	0.010	0.012	0.000	0.002	0.000	0.003	0.002	0.000	0.000	0.000	0.001	0.006	0.002
Na	0.134	0.164	0.119	0.138	0.104	0.037	0.139	0.112	0.053	0.120	0.107	0.147	0.113	0.101	0.106	0.124	0.125
K	1.642	1.736	1.588	1.708	1.506	1.206	1.765	1.825	2.003	1.873	1.999	1.982	1.866	1.877	1.822	1.905	1.900
Cr	0.004	0.001	0.000	0.003	0.003	0.000	0.000	0.003	0.002	0.008	0.000	0.000	0.002	0.005	0.001	0.007	0.003
Total	15.687	15.699	15.558	15.714	15.382	15.389	15.550	15.671	15.766	15.660	15.695	15.795	15.616	15.563	15.549	15.721	15.656
*Total Fe as FeO																	
Numbers of ions on the basis of 22 O																	
Si	5.438	5.502	5.447	5.395	5.727	5.418	5.412	5.321	5.334	5.215	5.319	5.271	5.270	5.319	5.334	5.167	5.187
Al^{IV}	2.562	2.498	2.553	2.605	2.273	2.582	2.588	2.679	2.666	2.785	2.681	2.729	2.730	2.681	2.666	2.833	2.813
sum T	8.000	8.000	8.000	8.000	8.000	8.000	8.000	8.000	8.000	8.000	8.000	8.000	8.000	8.000	8.000	8.000	8.000
Al^{VI}	0.720	0.692	0.867	0.701	0.913	0.843	0.807	0.795	0.716	0.776	0.734	0.552	0.791	0.820	0.861	0.723	0.767
Cr	0.004	0.001	0.000	0.003	0.003	0.000	0.000	0.003	0.002	0.008	0.000	0.000	0.002	0.005	0.001	0.007	0.003
Ti	0.119	0.153	0.138	0.160	0.101	0.102	0.292	0.238	0.236	0.337	0.332	0.357	0.342	0.354	0.317	0.345	0.377
Fe^{2+}	1.327	1.835	1.888	2.319	1.429	1.248	2.680	2.572	3.715	2.712	2.385	2.895	2.531	2.505	2.753	2.739	2.698
Mn	0.049	0.003	0.023	0.000	0.033	0.019	0.001	0.004	0.031	0.024	0.040	0.040	0.028	0.039	0.014	0.040	0.035
Mg	3.684	3.115	2.933	2.683	3.284	3.922	1.866	2.119	1.010	1.807	2.097	1.823	1.943	1.862	1.674	1.830	1.747
sum Y	5.904	5.799	5.850	5.866	5.763	6.134	5.646	5.732	5.710	5.664	5.587	5.667	5.637	5.585	5.620	5.685	5.629
Ca	0.007	0.000	0.001	0.001	0.010	0.012	0.000	0.002	0.000	0.003	0.002	0.000	0.000	0.000	0.001	0.006	0.002
Na	0.134	0.164	0.119	0.138	0.104	0.037	0.139	0.112	0.053	0.120	0.107	0.147	0.113	0.101	0.106	0.124	0.125
K	1.642	1.736	1.588	1.708	1.506	1.206	1.765	1.825	2.003	1.873	1.999	1.982	1.866	1.877	1.822	1.905	1.900
sum X	1.783	1.900	1.709	1.848	1.619	1.255	1.904	1.939	2.056	1.995	2.108	2.129	1.979	1.978	1.929	2.036	2.027
Total	15.687	15.699	15.558	15.714	15.382	15.389	15.550	15.671	15.766	15.660	15.695	15.795	15.616	15.563	15.549	15.721	15.656
X_{Mg}	0.74	0.63	0.61	0.54	0.70	0.76	0.41	0.45	0.21	0.40	0.47	0.39	0.43	0.43	0.38	0.40	0.39
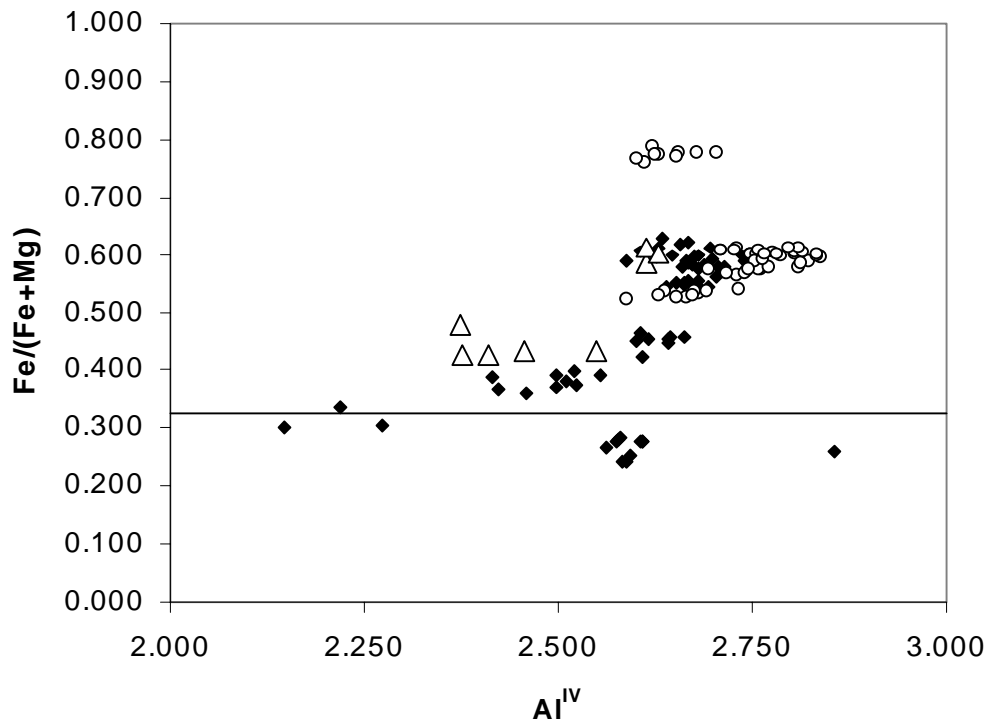
FIGURE 5. Chemical composition of the biotite for pelitic schists from the Silgará Formation in the Mutiscua area, central Santander Massif. Open triangles and circles indicate biotite from the upper and lower sillimanite zones, respectively; black rombs indicate biotite from the staurolite-kyanite zone.

temperatures were calculated in the Bucaramanga Gneiss unit near a migmatite zone (between California and Vetas towns). The temperature conditions range from 630 to 704°C in the staurolite-kyanite zone, and from 690 to 727°C in the sillimanite zone.

According to the geobarometry results, the metamorphic pressure conditions range from 5.0 to 9.5 kbar in the staurolite-kyanite zone, and from 6.6 to 7.5 kbar in the sillimanite zone.

Reaction history

To reconstruct the reaction history of the metamorphic rocks in the CSM, special attention was focussed on mineral assemblages, their relationships with respect to the deformation history, reaction textures and mineral chemistry, using the chemical system K_2O-FeO-MgO-Al_2O_3 -SiO_2-H_2O, which is referred here to as the KFMASH system (see FIGURE 7). The petrogenetic grid of Spear and Cheney (1989) will be used for discussion because provides an internally consistent framework and incorporates the effect of Fe-Mg solid solution behavior in all phases, and agrees well with the sequence of mineral reactions found in the metamorphic rocks of the Santander Massif, under intermediate pressure conditions, which are described below.

In the staurolite-kyanite zone there is textural evidence to support the first appearance of kyanite "*kyanite-in isograd*" in low-Al pelitic rocks such as the Silgará Formation, by the polymorphic reaction

(1) And = Ky

Staurolite is found in pelitic and/or semipelitic rocks with unsuitable composition to form chloritoid. Therefore, the following discontinuous reaction may be very important in the production of staurolite:

(2) Grt + Ms + Chl = St + Bt + Qtz + H_2O,
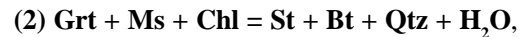
which is a major reaction because marks the first appearance of the staurolite + biotite assemblage and therefore the first appearance of staurolite "*staurolite-in isograd*". On the other hand, garnet has been partially resorbed by this reaction and a significant amount of chlorite will be removed along with the production of abundant staurolite and new biotite. Garnet sometimes occur as inclusions in staurolite porphyroblasts, which show a post-tectonic character respect to garnet, although pre-tectonic respect to the main foliation of the rock, indicating the occurrence of this reaction. Chlorite is relatively rare in the staurolite zone, except as a retrograde phase.

TABLE 8. Representative chemical compositions of plagioclase from metapelitic rocks of the Silgará Formation in the central Santander Massif. PS: Pelitic Schists. inc.Grt: inclusion in garnet.

Lithology	PS	PS	PS	PS	PS	PS	PS	PS	PS
Sample No.	PCM-20	PCM-21	PCM-47	PCM-49	PCM-618	PCM-651	PCM-701	PCM-702	PCM-953
Analysis No.	1	1	3	1	3	13	1	1	29
Weight %	rim	rim	rim	core	inc. Grt	mantle	rim	rim	rim
SiO_2	65.65	52.60	62.04	58.33	58.31	60.08	67.23	67.68	63.58
TiO_2	0.00	0.00	0.02	0.00	0.00	0.00	0.02	0.00	0.00
Al_2O_3	21.99	29.91	23.18	26.39	25.28	24.95	19.66	19.80	21.95
FeO*	0.00	0.06	0.05	0.00	0.28	0.04	0.00	0.03	0.05
MnO	0.01	0.02	0.00	0.00	0.00	0.00	0.01	0.00	0.00
MgO	0.00	0.00	0.01	0.00	0.01	0.00	0.01	0.00	0.00
CaO	2.01	12.22	4.79	8.53	7.03	7.08	0.55	0.74	3.14
Na_2O	10.26	4.38	9.05	6.78	7.62	7.53	11.52	10.37	9.97
K_2O	0.11	0.09	0.14	0.09	0.15	0.13	0.12	0.10	0.36
Cr_2O_3	0.00	0.00	0.00	0.01	0.00	0.01	0.00	0.00	0.00
Total	100.02	99.28	99.27	100.12	99.28	99.81	99.12	98.71	99.06
Cations per 8 O									
Si	2.880	2.397	2.771	2.606	2.651	2.681	2.970	2.987	2.837
Ti	0.000	0.000	0.001	0.000	0.000	0.000	0.001	0.000	0.000
Al	1.137	1.607	1.220	1.389	1.341	1.312	1.023	1.030	1.155
Fe^{2+}	0.000	0.002	0.002	0.000	0.011	0.001	0.000	0.001	0.002
Mn	0.000	0.001	0.000	0.000	0.000	0.000	0.000	0.000	0.000
Mg	0.000	0.000	0.000	0.000	0.000	0.000	0.001	0.000	0.000
Ca	0.094	0.597	0.229	0.408	0.339	0.339	0.026	0.035	0.150
Na	0.872	0.387	0.783	0.587	0.665	0.651	0.987	0.887	0.862
K	0.006	0.005	0.008	0.005	0.009	0.007	0.007	0.005	0.021
Cr	0.000	0.000	0.000	0.000	0.000	0.000	0.000	0.000	0.000
Total	4.990	4.995	5.014	4.996	5.016	4.992	5.015	4.945	5.027
*Total Fe as FeO									
Numbers of ions on the basis of 8 O									
Ternary feldspar composition (%)									
Anorthite	9.70	60.36	22.47	40.80	33.47	33.95	2.56	3.77	14.53
Albite	89.70	39.12	76.75	58.71	65.66	65.31	96.75	95.66	83.48
K-feldspar	0.60	0.52	0.78	0.49	0.86	0.74	0.68	0.58	1.99
X_{An}	0.10	0.61	0.23	0.41	0.34	0.34	0.03	0.04	0.15

According to Spear (1993), it is very probable that all chlorite and partially staurolite were consumed in these type of rocks, producing a new generation of biotite and the first appearance of kyanite by the reaction:

(3) St + Chl + Ms = Ky + Bt + H_2O
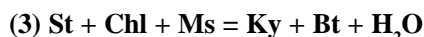
In the transition from the staurolite-kyanite zone to the sillimanite zone as staurolite becomes less abundant, preserved as inclusions or corroded relics in muscovite, a first generation of sillimanite appears within muscovite inmediately adjacent to garnet and occurs as aggregates of fibrolite, which may be together or penetrate biotite or quartz grains. Fibrolite is probably the result of a tie-line switching reaction that also produces biotite. In rocks that contain both kyanite and sillimanite, direct textural evidence for the polymorphic inversion from kyanite to sillimanite is rare. Instead, it occurs as clusters of minute, needle-shaped crystals embedded in biotite or quartz.
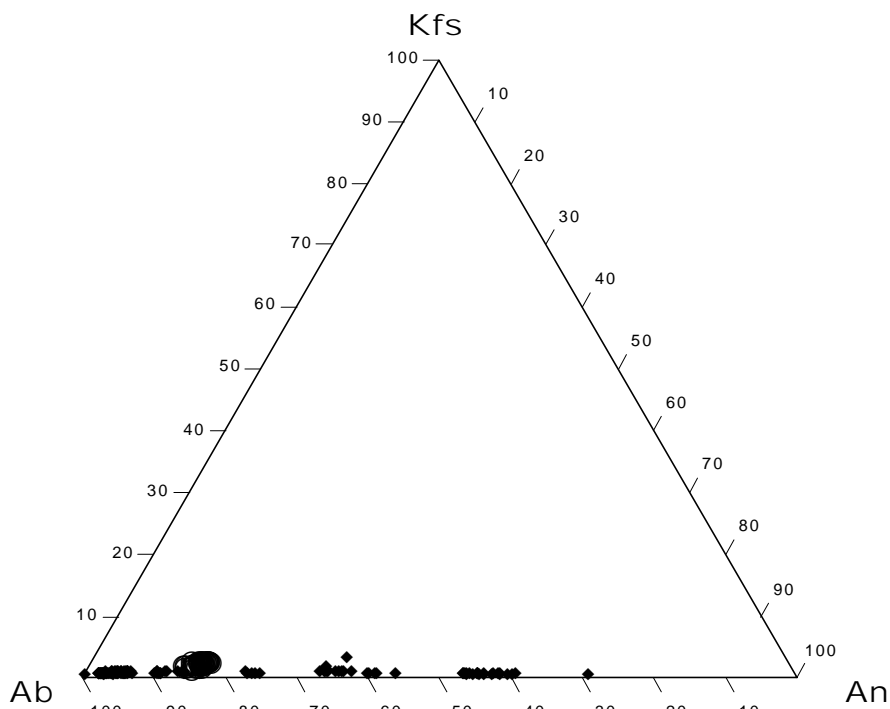
FIGURE 6. Chemical composition of the plagioclase for pelitic rocks from the Silgará Formation in the Mutiscua area, central Santander Massif. Open circles indicate plagioclase from the lower sillimanite zone; black rombs indicate plagioclase from the staurolite-kyanite zone.

In the sillimanite zone, according to Yardley (1977), sillimanite could appear as result of the univariant reaction:

(4) St + Ms + Qtz = Sil + Grt + Bt + H₂O,
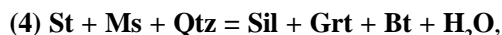
which marks the first appearance of sillimanite (fibrolite) and is very important in the disappearance of staurolite and is the terminal stability reaction for staurolite on the petrogenetic grid.

In the case of garnet was not involved in the consumption of staurolite, this mineral reacts by the following reaction: $St + Ms + Qtz = Al_2SiO_5 + Bt + H_2O$. Garnet Chemical zoning and sillimanite inclusions in muscovite and quartz may indicate decrease in pressure after the formation of sillimanite by this reaction and during staurolite-consuming reactions (increasing temperature).

We may deduce from a series of textural relationships in metamorphosed pelitic rocks that kyanite reacted to form sillimanite by the polymorphic reaction:

(5) Ky = Sil

In the CSM has been possible to establish a higher metamorphism than that reported in the typical Barrovian zonal scheme, because the thermal-peak of metamorphism

in the migmatite zone (e.g. sample PCM-156, Bucaramanga Gneiss unit) could be aproximately of 727°C at a pressure of 7.4 kbar, which are appropiate conditions to melt a metapelitic rock. Some authors (e.g., Le Breton & Thompson, 1988; Vielzeuf & Holloway, 1988) discuss about the pelite melting and it has been experimentally shown that liquids produced by the melting of metapelitic rocks are probably not saturated with respect to H_2O (*vapor absent melting*). In these rocks minerals such as muscovite and biotite are the best candidates for vapor absent melting, because the H_2O released by the dehydration of these minerals can react with quartz and feldspar to produce melts of granitic composition. According to Spear (1993), the elimination of muscovite can be attributed to either dehydration or melting reactions. At pressures between ≈3 and 14 kbar melting is favoured over dehydration and, therefore, muscovite should dehydrate first, producing an initial quantity of melt, by the following vapor absent melting reaction:

(6) Ms + Pl + Qtz = Bt + Kfs + Al₂SiO₅ + melt
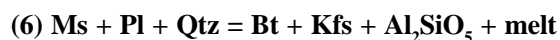
Retrograde reactions are mainly observed in the staurolite-kyanite zone, which include partial replacement of garnet by chlorite and/or biotite along cracks; heavily corroded core of aluminium-rich silicates such as staurolite are enclosed by sericite and chlorite; biotite and amphibole

are replaced by chlorite, although amphibole is sometimes replaced by biotite, and feldspar is partly replaced by sericite or caolinite. Additional evidence of retrograde metamorphism is observed in biotite that shows ilmenite exsolution. Needle-shaped crystals of ilmenite occur in the three directions within biotite. It is known that the quantity of Ti component of biotite increases with increasing metamorphic grade. Therefore, ilmenite may form out of the excess quantity of Ti expelled from biotite during retrograde metamorphism.

P-T path

We have delineated the tectono-metamorphic evolution of the CSM metamorphic rocks along a P-T path (FIGURE 7) as a function of relative time during a continent-continent collision model, which has been constrained by mineral reaction history and thermobarometric calculations. It may represent a crustal sequence that has been considerably heated, along with increasing pressure conditions, although it is not clear that addition of magmas is contributing to this heating. The tectonic transport of the metamorphic rocks in the CSM occurred along a clockwise pressure-temperature path, which is characteristic for the metamorphic evolution of rocks from most orogenic belts. The inferred P-T path suggests that during the tectonic transport these rocks may have undergone burial during the initial stages of collision. They were buried to its maximum depth at P_{peak}, reflecting a crustal shortening and thickening, and an increasing depth is accompanied by an increasing pressure, which is accompanied by a first stage of deformation (D_1) and development of S_1, leading to a syn-collisional prograde metamorphic event (D_2). A second stage of deformation (D_2) produces a S_2 schistosity associated to thrusting, before reaching the maximum pressure conditions. The tectonic transport between t_3 and t_4 does not increase the thickness of the crust, and pressure does not remain constant, based on the chemical zoning of garnet (from grossular distribution). The thickened crust is uplifted slowly and erosion tends to restore the original crust, which is characterized by decompression, new mineral growth and movement along S_3 (strain slip cleavages) during D_3 from t_3 to t_1. As initial uplift rates are slow compared with heat transport rates, these metamorphic rocks will be affected by a continued increasing temperature during uplift until to reach the position at T_{peak} (maximum temperature), from which these rocks will experience cooling, accompanied by retrograde metamorphism that is suggested from rehydration reactions very often do not terminate, and assemblages from least hydrated state have been preserved as relicts (t_5). During the retrograde stage occurred the emplacement of orthogneiss masses of the Orthogneiss. The infiltration of water for retrograde metamorphism is intruded to the rocks by late deformation events. Anyway, at this moment the volume element has not returned to its original depth position and therefore the stable steady state geotherm has not been re-established. Note that the maximum temperature is not reached at the maximum pressure, and, therefore, the temperature-peak conditions occurs after maximum burial, which has been suggested by Ríos (1999) from the chemical zoning of grossular in garnet, because grossular component shows a maximum content in the mantle, which is interpreted as reflecting the pressure-peak conditions during garnet growth before reaching the temperature-peak conditions.

DISCUSSION

Metamorphism in the CSM has occurred under conditions of high-temperature and medium-pressure (Barrovian type metamorphism). The CSM metamorphic rocks have followed a clockwise pressure-temperature path, which is characteristic for the metamorphic evolution of rocks from most orogenic belts, and could reflects a typical region that have been undergone crustal thickening by continental collision.

TABLE 9. P-T conditions of the central Santander Massif metamorphic rocks.

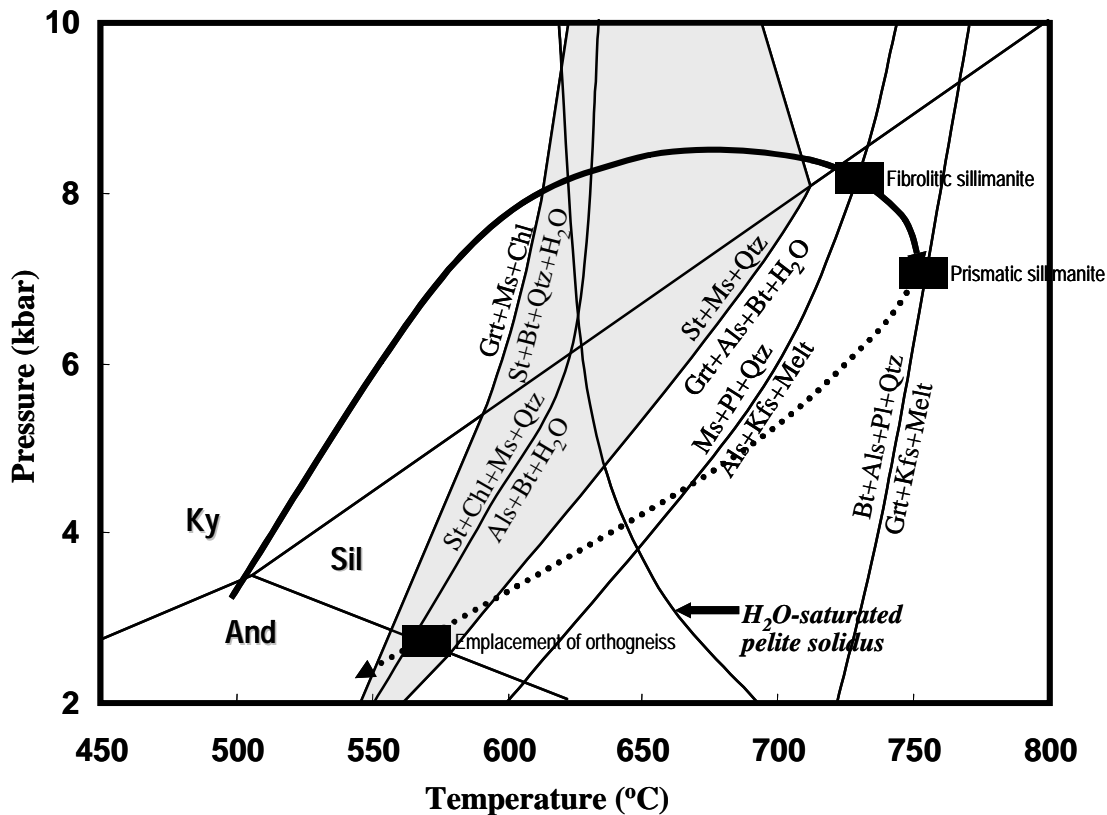| Study Area	Central region				
Metamorphic zone	Staurolite-Kyanite	Staurolite-Kyanite	Staurolite-Kyanite	Sillimanite	Sillimanite
Sample N°	PCM-28	PCM-16	PCM-618	PCM-855	PCM-156
Temperature, (°C)	630	697	704	690	727
Pressure, (Kilobars)	9.5	5.0	8.3	7.5	6.6

FIGURE 7. P-T path followed by the metamorphic rocks in the central Santander Massif. The Al_2SiO_5 triple point after Holdaway (1971), and the stability field of staurolite after Bucher & Frey (1994). The shadow area shows the coexistence of St+Qtz. Reactions for the vapor absent melting and H_2O-saturated pelite solidus after Spear (1993).

Recent interpretations of the metamorphic history of the Santander Massif in different regions have been proposed by Ríos (1999), Ríos and Takasu (1999), Montenegro y Barragán (1998), García y Ríos (1999), Ríos *et al*. (2003) based on fabric relationships. Restrepo-Pace (1995) and Cardona (2003) report ages in the metamorphic rocks of the Santander Massif, which along with the thermobarometric estimates, the textural relationships and the P-T path obtained in this study let to discuss the different models that explain the regional tectonics in order to propose a model of the tectono-metamorphic evolution of the CSM.

The tectonic evolution of the nortern Andes has been explained during the last years from terrane accretions (Toussaint, 1993), continental collisions (Restrepo-Pace, 1995) or accretion of small blocks that joined to another southamerican blocks formed the Rodinia supercontinent (Cordani, et al, 2003).

Radiometric ages determinations indicate that the oldest rocks of the Santander Massif correspond to the BG of Precambrian age. Goldsmith *et al*. (1971) reported a K-

Ar hornblende age of 945±140 Ma. Restrepo-Pace (1995) defines a cooling age aproximately of 800 Ma, which is established from complex spectra of Ar/Ar. Recently, Cardona (2003) reports U/Pb ages (SHRIMP in zircons) of 1450-1550 Ma that will correspond to the age of the protolith of the BG, and 1140-1190 Ma that will reflect the age of the first metamorphic event of this unit. These data are very well correlated with the Sm/Nd whole-rock age of 1160 Ma, which have been obtained by the same author for the metamorphism of the BG.

These Precambrian ages are very well correlated with those obtained in the Garzón Massif, Sierra Nevada de Santa Marta and Guajira Peninsula in the colombian territory, as well as in the Canadian Shield and the Oaxacan Complex in México.

The Precambrian ages vary between 945 and 1100 Ma, when a granulitic belt was developed during the Greenville orogeny in the Canadian Shield and during the Nickeriense-Orinoquiense orogeny in South América. According to Priem (1989), the Nickeriense-Orinoquiense orogeny reflects a continental collision between the western margin

of the Guyana Shield and the eastern margin of the Canadian Shield. However, Restrepo-Pace (1995) and Aleman and Ramos (2000) also mention a close relationship between the Guyana Shield and the Oaxacan Complex in the southeast of México.

Cordani (2003) and Cardona (2003) propose a collision between continental blocks, which were accreted to constitute Rodinia, taking into account the geochemistry and geochronology data similarity found between the Santander Massif rocks and the Proterozoic basement of the Amazon Craton, and the Canadian Shield (Greenville orogeny).

The ages (1140-1190 Ma and 1100-900 Ma) obtained for the BG will indicate a collision between local terrenes (continental blocks, arcs) and a continental collision between western margin of Gondwana and the eastern margin of Laurentia, respectively.

Respect to the SF, scarce isotopic data do not let to precise the age of its metamorphism, however, we let to make an aproximation of this age from some isotopic data, the field relationships between the SF and the Bucaramanga Gneiss and Orthogneiss units and from deformation and metamorphic events that have affected to this metamorphic unit (SF).

Restrepo-Pace (1995) report a U/Pb zircon age of 480 Ma for the emplacement of syntectonic intrusives (orthogneiss), which is very similar to the K-Ar hornblende age of 413±30 Ma (metadiorite), K-Ar muscovite age of 457±13 Ma (pegmatite in the BG), and Rb-Sr whole-rock age of 450±80 Ma (gneissic granite), reported by Goldsmith et al. (1971), suggesting a magmatic event in the late Ordovician or early Silurian, and the Santander Massif, and the metamorphism of the SF y O may have occurred at this time (Goldsmith et al., 1971; Restrepo-Pace, 1995).

Sedimentation and metamorphism of the SF may occur in the range 750-470 Ma, which is reported by Restrepo-Pace (1995) as a continental breaking stage with development of a carbonate-clastic sequence along the continental margin. A tectono-thermal event around 470 Ma has been recognized in different regions of South América (Puna, Argentina, southeastern Bolivian Andes), which is known as Famatinian orogeny, during which a high temperature and middle pressure and an emplacement of numerous syntectonic intrusions occurred. The Famatinian orogeny can be correlated with the Caparonensis orogeny in the Mérida Andes that occurs

in 470-480 Ma. We consider that the age of 450-480 Ma corresponds to the syntectonic emplacement and metamorphism of the O unit, which occurred during the retrograde metamorphism stage of the SF, during its exhumation. Metamorphism of the Silgará Formation may be correlated with collision between continental blocks, according to the clockwise P-T path and the transition kyanite-sillimanite determined for the CSM in this study.

The Ar/Ar ages of cooling in muscovite and biotite next to 200 Ma are reported by Restrepo-Pace (1995) for the SF in the southwestern Santander Massif, and coincide with those obtained by Cardona (2003) using the same method for biotite and amphibole in rocks of the BG. On the other hand, Goldsmith et al. (1971) also reported K-Ar whole-rock ages of 221±8 Ma and 198±8 Ma from phyllites of the SF. These ages are similar to those obtained by Dörr et al. (1995); Boinet et al. (1985); Goldsmith et al. (1971) in different intrusive bodies that cut the metamorphic units. For this reason, ages around 200 Ma reported for the metamorphic rocks correspond to a thermal perturbation event due to the emplacement of calcalkaline plutons.

Therefore, according to the isotopic data mentioned above, we can preliminarly conclude that the metamorphism in the CSM reflects important events related to the Gondwana-Laurentia collision (BG), a posible continental breaking (SF), and a orogenic event corresponding to the Famatinian (Southern Andes) and Caparonensis (Mérida Andes) orogenies. However, these preliminar considerations should be stated clearly and accurately and complemented with more isotopic data specially respect to the SF and O metamorphic rocks.

ACKNOWLEDGEMENTS

Discussions with the Reseach Group in Mineralogy, Petrology and Geochemestry "MINPETGEO" aided our understanding of the Santander Massif geology. The manuscript has benefited from the constructive reviews. The authors are grateful two anonymous reviewers.

REFERENCES

Aleman, A., and Ramos, V. A. (2000). Northern Andes. In: Cordani, U.G., et al. (Eds), Tectonic evolution of South America. 31st Internacional Geological Congress, Rio de Janeiro, pp. 453-480.

Bence, A., and Albee, A. (1968). Empirical correction factors for the electron microanalysis of silicates and oxides. Journal of Geology, Vol. 76, pp. 382-403.

Berman, R. (1997) Programm TWQ version 2.02. In: http://www.gis.nrcan.gc.ca/twq.html

Boinet, T., Bourgois, J., Bellon, H., and Toussaint, J.F. (1985). Age et repartition du magmatism premesozoique des Andes de Colombie. Comptes rendus hebdomadaires des séaces de L'Académie des Sciences. Serie D: Sciences Naturalles, Vol. 300(II), pp. 445-450.

Cardona, A. (2003). Correlacoes entre fragmentos do embasamento Pre-Mesozoico da terminacao setentrional dos Andes Colombianos, com base em datos isotopicos e geocronologicos. Dissertacao de Mestrado, Universidade de Sao Paulo, Instituto de Geociencias, 149 pp.

Castellanos, O.M. (2001). Chemical composition of the rock-forming minerals in the Silgará formation and P-T conditions in the Mutiscua area, Santander Massif, Eastern Cordillera, Colombia. Master Thesis, Shimane University, Matsue (Japan), 146pp.

Castellanos, O.M., Ríos, C.A., and Takasu, A. (2004). Chemically sector-zoned garnets in the metapelitic rocks of the Silgará Formation in the central Santander Massif, Colombian Andes: occurrence and growth history. Boletín de Geología, Vol. 26(42), pp.9-18.

Chinner, G.A. (1961). The origin of sillimanite in Glen Clova, Angus. Journal of Petrology, Vol. 2(3), pp. 312-323.

Cordani, U.G., Cardona, A., Jiménez, D.M., and Liu, D. (2003). Did the Precambrian basement inliers of northern Colombia play any role in Rodinia´s formation?. Memorias Resumenes IX Congreso Colombiano de Geología, Medellín, pp. 34.

Dörr, W., Grösser, J., Rodriguez, G., and Kramm, U. (1995). Zircon U-Pb age of the Paramo Rico tonalite-granodiorite, Santander Massif (Cordillera Oriental, Colombia) and its geotectonic significance. Journal of South American Earth Sciences, Vol. 8(2), pp. 187-194.

García, C.A., y Ríos, C.A. (1997). Mineralogía y Petrografía de las Metamorfitas al Oeste de Pamplona (Norte de Santander), Colombia". Memorias del XVI Curso Internacional de Postgrado en Metalogenia. Sesión Ponencias. Universidad Central del Ecuador (Quito), pp. 77-93.

García, C.A., y Castellanos, O.M. (1998). Petrografía de la Formación Silgará en la Cordillera Oriental, Colombia. X Congreso Latinoamericano de Geología, Buenos Aires, Argentina, Memorias, T.2, pp. 263-268.

García, C.A., y Ríos, C.A. (1999). Metamorfismo y metalogenia asociada del Macizo de Santander, Cordillera Oriental, Colombia. Informe final Proyecto de Investigación. Universidad Industrial de Santander-Colciencias, p. 191.

García, C.A., y Campos, N.O. (2000). Composición química y mineralogía de las biotitas metamórficas del sector central del Macizo de Santander, Colombia. Boletín de Geología, Vol. 22 (37), pp. 18-27.

Goldsmith, R., Marvin, R.F., and Mehnert, H.H. (1971). Radiometric ages in the Santander Massif, eastern Cordillera, Colombian Andes. U.S. Geological Survey Professional Paper, Vol. 750-D, pp. D41-D49.

Gordon, T., Aranovich, L., and Fed'kin, V. (1994). Exploratory data analysis in thermobarometry: An example from the Kisseynew sedimentary gneiss belt, Manitoba, Canada. American Mineralogist, Vol. 79, pp. 973-982.

Holdaway, M.J. (1971). Stability of andalusite and the aluminum silicate phase diagrams. American Journal of Science, Vol. 271, pp. 97-131.

Inger, S., and Harris, N. (1992). Tectonothermal evolution of the High Himalayan Crystalline Sequence, Langtang Valley, northern Nepal. Journal of Metamorphic Geology, Vol. 10, pp. 439-452.

Julivert, M. (1958). La morfoestructura de la zona de mesas al SW de Bucaramanga. Boletín de Geología / Universidad Industrial de Santander (Colombia), Vol. 1, pp. 7-44.

Julivert, M. (1959). Geología de la vertiente W del Macizo de Santander en el sector de Bucaramanga. Boletín de Geología/Universidad Industrial de Santander (Colombia), Vol. 3, pp. 15-34.

Julivert, M. (1961a). Las estructuras del valle medio del Magdalena y su significación. Boletín de Geología/ Universidad Industrial de Santander (Colombia), Vol. 6, pp. 33-52.

Julivert, M. (1961b). Geología de la vertiente W de la Cordillera Oriental en el sector de Bucaramanga. Boletín de Geología / Universidad Industrial de Santander (Colombia), Vol. 8, pp. 39-42.

Julivert, M. (1963). Nuevas observaciones sobre la estratigrafía y tectónica del Cuaternario de los alrededores de Bucaramanga. Boletín de Geología / Universidad Industrial de Santander (Colombia), Vol. 3, pp.15-34.

Julivert, M. (1970). Cover and basement tectonics in the Cordillera Oriental of Colombia, South America, and a comparison with some other folded chains. Geological Society American Bulletin, Vol. 81, pp. 3623-3643.

Kretz, R. (1983). Symbols for rock-forming minerals. American Mineralogist, Vol. 68, pp. 277-279.

Le Breton, N., and Thompson, A.B. (1988). Fluid-absent (dehydration), melting of biotite in metapelites in the early stages of crustal anatexis. Contributions to Mineralogy and Petrology, Vol. 99, pp. 226-237.

Maya, M. (1997). Distribución de facies y edad de las rocas metamórficas en Colombia. Ingeominas, Medellin, p.59.

Montenegro, G., y Barragán, M. (1999). Metamorfismo y Evolución Metamórfica del área comprendida entre los municipios de Vetas (Santander) y Mutiscua (Norte de Santander). Tesis de Pregrado, Universidad Industrial de Santander, Bucaramanga (Colombia).

Ordoñez, J.C. (2003). Petrology and geochemistry of the granitoids at the Santander Massif, Eastern Cordillera, Colombian Andes. Master Tesis, Shimane University, Matsue (Japan), 150pp.

Priem, H.N.A., Kroonenberg, S.B., Boelrijk, N.A.I.M., and Hebeda, E.H. (1989). Rb-Sr evidencefor the presence of a 1.6 Ga. Basement underlying the 1.2 Ga. Garzón-Santa Marta Granulite Belt in the Colombian Andes. Precambrian Research, Vol. 42, pp. 315-324.

Restrepo-Pace, P. (1995). Late Precambrian to Early Mesozoic tectonic evolution of the Colombian Andes, based on new geochronological, geochemical and isotopic data. Ph.D Thesis, University of Arizona, 195pp.

Ríos, C.A. (1999). Chemical Compositions of the Constituent Minerals and P-T Conditions of the Low-grade Silgará Formation Metamorphic Rocks in the Santander Massif, Eastern Cordillera, Colombian Andes. Master Tesis, Shimane University, Matsue (Japan), 207 pp.

Ríos, C.A., and Takasu, A. (1999). Chemical zoning of garnet from the low-grade metamorphic rocks of the Silgará Formation, Santander Massif, Eastern Cordillera (Colombian Andes). Geosciences Reports of Shimane University, Vol. 18, pp. 97-107.

Ríos, C.A., García, C.A., and Takasu, A. (2003). Tectono-metamorphic evolution of the Silgará Formation metamorphic rocks in the southwestern Santander Massif, Colombian Andes. Journal of South American Earth Science, Vol. 16, pp. 133-154.

Ríos, C.A., y García, C.A. (2001). Primera ocurrencia de los tres polimorfos de Al_2SiO_5 en las rocas metapelíticas de la Formación Silgará, Región Suroccidental del Macizo de Santander. Boletín de Geología, Vol. 23 (38), pp. 51-59.

Schäfer, J., Grösser, J., and Rodríguez, G. (1998). ?Proterozoic Formation Silgará, Cordillera Oriental, Colombia: metamorphism and geochemistry of amphibolites. Zbl. Geol. Paläont. Teil I, (3-6), Stuttgart, pp. 531-546.

Spear, F.S., and Cheney, J.T. (1989). A petrogenetic grid for pelitic schists in the system SiO_2-Al_2O_3-FeO-MgO-K_2O-H_2O. Contributions to Mineralogy and Petrology, Vol. 101, pp. 149-164.

Spear, F.S. (1993). Metamorphic Phase Equilibria and Pressure-Temperature-Time Paths. Mineralogical Society of America, Washington, DC, 799pp.

Toussaint, J.F. (1993). Evolución geológica de Colombia: Precámbrico Paleozoico. Pub. Esp. Geol. Univ. Nacional, Medellín, 208pp.

Vielzeuf, D., and Holloway, J.R. (1988). Experimental determination of fluid-absent melting relations in the pelitic system: consequences from crustal differentiation.

Contributions to Mineralogy and Petrology, Vol. 98, pp. 257-276.

Ward, D.E., Goldsmith, R., Cruz, B.J., Jaramillo, C.L., y Vargas, L.R. (1970). Mapa Geológico del Cuadrángulo H-13, Pamplona, Colombia. Ingeominas.

Ward, D.E., Goldsmith, R., Cruz, B.J., Jaramillo, C.L., y Restrepo, H. (1973). Geología de los Cuadrángulos H-12, Bucaramanga y H-13, Pamplona, Departamento de Santander. U.S. Geological Survey e Ingeominas. Boletín Geológico, Vol. 21(1-3), 132pp.

Yardley, B.W.D. (1977). The nature and significance of the mechanism of sillimanite growth in the Connemara schists, Ireland. Contributions to Mineralogy and Petrology, Vol. 65, pp. 53-58.